Ragni Maria Skjervold Olsson

# Characterization of cerium oxide nanoparticles and their toxicity in *Caenorhabditis elegans*

June 2019

Master's thesis

Master's thesis

2019

Ragni Maria Skjervold Olsson

**NTNU**
Norwegian University of
Science and Technology
Faculty of Natural Sciences
Department of Physics

**NTNU**
Norwegian University of
Science and Technology

**NTNU**
Norwegian University of
Science and Technology

# NTNU
## Norwegian University of Science and Technology

# Characterization of cerium oxide nanoparticles and their toxicity in *Caenorhabditis elegans*

## Ragni Maria Skjervold Olsson

*Phase contrast image of an adult hermaphrodite C. elegans. A recently released egg and a lump of E. coli is seen close to the nematode. Image by the author.*

# Preface

This thesis is the final part of a master degree in Nanotechnology at the Norwegian University of Science and Technology (NTNU). It was performed during the spring 2019, and is a continuation of a project thesis performed during the autumn 2018. A few results from the project thesis are included for comparison, and this is emphasized in the text where relevant. A few written parts are also similar between the two theses. The section *Sammendrag* is a Norwegian translation of the section *Abstract*, and does not contain any new information for the English reader.

Oslo, June 2019

*Ragni Maria Skjervold Olsson*

# Abstract

The objectives of this thesis were to investigate the toxicity of $CeO_2$ nanoparticles in the model organism *C. elegans*, and to study the mechanisms of toxicity behind such effect. Although $CeO_2$ nanoparticles are used in a range of applications and end up in the environment, their ecotoxicological risk potential and possible toxic mechanisms are not well understood. Existing literature reports both toxic and beneficial effects of $CeO_2$ nanoparticles, possibly due to the redox-potential of the nanoparticles. The present work was performed to gain further insight into the mechanisms behind these contradictory reports.

$CeO_2$ nanoparticles were firstly characterized with respect to size and charge. Wild type L1 stage larvae of *C. elegans* were then exposed to $CeO_2$ nanoparticles ($0.51 - 33$ mg/L) or $Ce^{3+}$ ($2 - 26$ mg/L), suspended in the standardized test medium moderately hard reconstituted water. After 96 h, nematode growth, fertility and reproduction was compared to controls. The cerium concentration was measured at the beginning and end of the test to assess the exposure conditions, and in stock suspensions at different time intervals to assess the degree of agglomeration and sedimentation. Nematode oxidative stress response was assessed by toxicity tests with transgenic strains of *C. elegans*; the reporter strain SOD-1 and the biosensor strain GRX. Different liquid media were tested for their effect on nematode growth.

The nanoparticle size distribution was assessed using transmission electron microscopy and nanoparticle tracking analysis, and the normal distributions were shown to have peak frequencies around 10 and 60 nm, respectively. The zeta potential of $CeO_2$ nanoparticles in the exposure medium was $-9.8$ mV. For $Ce^{3+}$ exposure, significant decrease in the growth of the nematodes was measured for 4 to 26 mg/L cerium. Fertility was significantly decreased from 12 to 26 mg/L cerium. Reproduction was significantly increased at 2 mg/L cerium, and significantly decreased for 4 to 26 mg/L cerium. $CeO_2$ nanoparticle exposure caused no significant change in growth or fertility. For reproduction, a significant decrease was shown at 4.1 and 8.0 mg/L cerium, but not for the higher concentrations of 16 or 33 mg/L cerium.

Inductively coupled plasma mass spectrometry showed that the exposure concentrations of cerium were close to the estimated concentrations, both at the beginning and end of the wild type toxicity test. Samples from nanoparticle stock suspensions showed a decrease in cerium concentration with time, and high variations between samples. This indicated that the suspension protocol produced unstable suspensions, with nanoparticle agglomeration and sedimentation. SOD-1 assays were affected by nematode culture issues, and no conclusions could be drawn based on the presented results. For GRX, there was no change in the oxidized over reduced ratio of glutathione after $Ce^{3+}$ exposure, but for $CeO_2$ nanoparticles a significant increase in the ratio was seen after 48 h exposure to 8.1 and 33 mg/L cerium. S-base with cholesterol produced the longest nematodes, followed by moderately hard reconstituted water and lastly moderately

hard reconstituted water with cholesterol.

This work has confirmed the potential toxic effect of $CeO_2$ nanoparticles in the environment. The results indicate a nano-specific toxic mechanism caused by the redox-potential of the nanoparticles. The effect is present at intermediate concentrations, and the lack of effect at higher concentrations is assumed to be due to increased nanoparticle agglomeration. Further work should focus on comprehensive characterization of the exposure conditions to gain further insight into the toxic mechanisms.

# Sammendrag

Målet med denne oppgaven var å undersøke toksisiteten av $CeO_2$ nanopartikler i modellorganismen *C. elegans*, og å undersøke de toksiske mekanismene for en slik effekt. Selv om $CeO_2$ nanopartikler brukes i en rekke kommersielle produkter og ender opp i miljøet, er deres økotoksikologiske risiko og mulige toksiske mekanismer ikke grundig forsket på. Eksisterende litteratur rapporterer om både toksiske og fordelaktige effekter av $CeO_2$ nanopartikler, muligens på grunn av nanopartiklenes redoks-potensiale. Arbeidet i denne avhandlingen ble utført for å få mer innsikt i mekanismene bak disse motstridende effektene.

$CeO_2$ nanopartikler ble først karakterisert med hensyn til størrelse og ladning. L1-stadium larver av *C. elegans* ble så utsatt for $CeO_2$ nanopartikler $(0,51 - 33$ mg/L) eller $Ce^{3+}$ $(2-26$ mg/L), suspendert i det standardiserte testmediet moderat hardt rekonstituert vann. Etter 96 timer ble vekst, fruktbarhet og reproduksjon sammenlignet mot kontroller. Ceriumkonsentrasjonen ble målt i begynnelsen og slutten av testen for å vurdere eksponeringsbetingelsene, og i stock suspensjoner ved forskjellige tidsintervaller for å vurdere graden av agglomerering og sedimentering av nanopartikler. Oksidativ stressrespons for nematodene ble vurdert ved å teste to transgene stammer av *C. elegans*; reporterstammen SOD-1 og biosensorstammen GRX. Ulike testsmedier ble testet for deres effekt på nematodevekst.

Størrelsesfordelingen av nanopartiklene ble undersøkt ved hjelp av transmisjonselektronmikroskopi og nanopartikkelsporingsanalyse, og normalfordelingene ble vist å ha toppfrekvenser på henholdsvis 10 og 60 nm. Zeta-potensialet for $CeO_2$ nanopartikler i eksponeringsmediet var -9,8 mV. For $Ce^{3+}$-eksponering ble signifikant reduksjon i nematodeveksten målt for 4 til 26 mg/L cerium. Fertiliteten ble signifikant redusert fra 12 til 26 mg/L cerium. Reproduksjonen økte signifikant ved 2 mg/L cerium, og minsket signifikant for 4 til 26 mg/L cerium. Eksponeringen av nanopartikler ga ingen signifikant endring i vekst eller fruktbarhet. For reproduksjon ble en signifikant reduksjon vist ved 4,1 og 8,0 mg/L cerium, men ikke for de høyere konsentrasjonene 16 eller 33 mg/L cerium.

Induktivt koblet plasma massespektrometri viste at eksponeringskonsentrasjonene av $Ce^{3+}$ var nær de estimerte konsentrasjonene, både ved begynnelsen og slutten av toksisitetstesten. Prøver fra stock suspensjonene av $CeO_2$ nanopartikler viste en reduksjon i ceriumkonsentrasjon med tiden, og høye variasjoner mellom prøvene. Dette indikerte at suspensjonsprotokollen ga ustabile suspensjoner, med agglomerering og sedimentering av nanopartikler. Toksisitetstesten for SOD-1 ble påvirket av problemer med nematodekulturen, og ingen konklusjoner kunne trekkes basert på de presenterte resultatene. For GRX var det ingen endring i forholdet mellom oksidert og redusert glutation etter $Ce^{3+}$ eksponering, men for $CeO_2$ nanopartikler ble en signifikant økning i forholdet observert etter 48 timers eksponering av 8,1 og 33 mg/L cerium. S-base med kolesterol produserte de lengste nematodene, etterfulgt av moderat hardt rekonstituert vann og til slutt moderat hardt rekonstituert vann med kolesterol.

Denne avhandlingen har bekreftet den potensielle giftige effekten av CeO$_2$ nanopartikler i miljøet. Resultatene indikerer en nano-spesifikk toksisk mekanisme forårsaket av nanopartiklenes redoks-potensiale. Effekten er tilstede ved mellomstore ceriumkonsentrasjoner, og mangelen på effekt ved høyere konsentrasjoner antas å skyldes økt agglomerering av nanopaertikler. Videre arbeid bør fokusere på omfattende karakterisering av eksponeringsforholdene for å få mer innblikk i de toksiske mekanismene.

# List of abbreviations

| | |
|---|---|
| **CAT** | Catalase |
| **CNT** | Carbon nanotube |
| **ddH$_2$O** | Double-distilled water |
| **EC** | Effect concentration |
| **ENM** | Engineered nanomaterial |
| **GFP** | Green fluorescent protein |
| **GPX** | Glutathione peroxidase |
| **GRX** | *C. elegans* biosensor strain jrIs2[Prpl-17::Grx1- roGFP2] |
| **GSH** | Glutathione |
| **GSSG** | Glutathione disulfide |
| **HSD** | Honestly Significant Difference |
| **ICP-MS** | Inductively coupled plasma mass spectrometry |
| **IS** | Ionic strength |
| **LB** | Lysogeny broth |
| **MHRW** | Moderately hard reconstituted water |
| **MHRW T** | Moderately hard reconstituted water with 0.2 % Tween 20 |
| **MHRW T 90** | 90 % moderately hard reconstituted water with 0.2 % Tween 20 and 10 % ddH$_2$O |
| **MOA** | Mechanism of action |
| **N2** | Wild type Bristol *C. elegans* strain |
| **NGM** | Nematode growth media |
| **NP** | Nanoparticle |
| **NTA** | Nanoparticle tracking analysis |
| **PAH** | Polycyclic aromatic hydrocarbon |
| **ROS** | Reactive oxygen species |
| **SD** | Standard deviation |
| **SOD** | Superoxide dismutase |
| **SOD-1** | *C. elegans* reporter strain GA508 wuls54[pPD95.77 sod::1GFP, rol-6(su1006)] |
| **TEM** | Transmission electron microscopy |

# Contents

# 1 Introduction

Research and applications within the field of nanotechnology are experiencing an impressive growth. Exciting possibilities have been identified in such diverse fields as medicine, electronics and materials science, and have been predicted to aid in solving some of the biggest problems of our time, including climate change and human disease [1, 2]. However, the increase in commercial applications of engineered nanomaterials (ENMs) is coupled with an increase in the release of ENMs into the environment. To minimize unwanted side effects, there is a need for thorough investigation of the released amounts of ENMs, their environmental fate and their potential toxicity for living organisms, including humans [3].

The unique properties of ENMs make risk assessment challenging. Unlike traditional bulk materials, the toxicity of ENMs is not only determined by the concentration, route of exposure and exposure time, but also by properties such as particle size and shape. The effect of surface chemistry, charge and coating become more prominent with the substantial increase in surface area to volume ratio [4, 5]. The widespread use of different ENMs with unique properties require new thinking in risk assessment and legislation. To enable this, there is a considerable need for more nanotoxicological research. This includes exposure assessments, toxicity assessments, and an extensive effort into understanding the mechanisms behind toxic effects. The aim of this master thesis is to contribute to filling this knowledge gap.

One ENM getting increased attention is cerium oxide nanoparticles (NPs). Despite the extensive use of cerium oxide NPs in applications such as fuel additives, catalytic converters and planarization media, and their confirmed release into the environment, the potential toxic effects are not well investigated [6–9]. Cerium oxide NPs have been reported to cause toxic effects in different cell cultures and model animals. However, beneficial effects have also been reported, and this contradiction is believed to originate from the redox-potential of the cerium oxide NPs [10].

In a review of the environmental behavior and toxic effects of cerium oxide NPs, Collin *et al.* list soil invertebrates, such as nematodes, as a suitable model organism for assessing the toxicity of cerium oxide NPs [6]. The nematode *Caenorhabditis elegans* (*C. elegans*) has been used extensively as a model organism since the 1970s, when Sydney Brenner suggested its potential for studying neural development [11]. The roundworm is around 1 mm long and transparent, with a short life cycle and a large number of offspring. These traits make it a valuable tool in a variety of research fields, including toxicology.

Due to the unique challenges of nanotoxicological assessments, the investigation of ENM toxicity without thorough characterization is of very limited value [12–14]. Investigation of the dynamical physicochemical properties of the NPs and the NP behavior in the exposure medium is paramount to be able to interpret the results, and to suggest which NP characteristics are responsible for the toxic effect. This is also valueable for the regulation of ENMs, which would

greatly benefit from the categorization of ENMs with similar toxic mechanisms of action (MOA).

In this work, the toxicity of $CeO_2$ nanoparticles was investigated in the nematode *C. elegans*. The $CeO_2$ nanoparticles were characterized, and the possible mechanism of toxicity investigated. Three hypotheses were formulated; I) Cerium oxide NPs are toxic to *C. elegans*, II) The toxic effect is caused by a disturbance in the cellular redox balance, and III) The toxic effect decreases for high concentrations due to extensive NP agglomeration.

# 2 Theory

## 2.1 Nanotoxicology

In the field of toxicology, it is common to organize toxic compounds into groups of chemicals with similar properties, such as metals, polycyclic aromatic hydrocarbons (PAHs) or radioactive isotopes. ENMs are no exception to this rule, even though it is a diverse group with in principle only the size limit as their common denominator. ENMs are materials with a size below 100 nm in at least one dimension, and include metals, metal oxides, polymers, and a variety of carbon materials such as graphene, fullerenes and carbon nanotubes (CNTs). The physical and chemical properties of many materials change drastically when one goes from bulk to nano-sized dimensions. There is a high background level of naturally occurring nanomaterials, but with the recent massive increase in research, production and new applications of ENMs, special interest has been directed towards the potential toxic effects of this fraction of nanomaterials [15].

ENM-induced toxicity can arise due to the inherent toxicity of the ENM or due to the enhancement of the toxic effect of other compounds [4]. Silver NPs are commonly used in consumer goods due to their antibacterial properties, and is also one of the most studied ENMs with respect to inherent toxic effects [16]. CNTs is an example of an ENM with the potential to enhance toxic effects of other compounds. CNTs can absorb PAHs, possibly affecting the availability, uptake, accumulation or toxicity of these chemicals to organisms. The factors contributing to a decrease or increase in observed toxicity are currently under investigation [17–20].

For NPs with inherent toxic properties, toxicity can be caused by a release of ions or by nano-specific mechanisms, or by a combination of several contributions. For compounds where the ionic forms show no toxic effect, or where the NPs are known to be inert, a nano-specific MOA can be assumed. Possible mechanisms of nano-specific toxicity include mechanical damage to cellular membranes or organism surface, agglomeration and bioaccumulation inside the organism, clumping of food due to agglomeration with the NPs, or a redox potential of the NP surface. The two terms aggregate and agglomerate will in this thesis be described solely by the term agglomerate, as recommended by Nichols *et al.* [21].

Assessing the toxicity of any compound is no easy task. For ENMs, the task is further complicated by the infinite amount of different varieties of the same material. For metal oxide NPs, properties such as size, shape, surface charge, stability, degree of agglomeration, pH value and the presence of natural organic matter (NOM) in the medium have been shown to affect toxicity [4, 5, 22–24]. Hence, it can be difficult or even impossible to compare results based on different types of nanomaterials.

For all types of materials, the steps of toxic risk assessment are 1) hazard identification, 2a) dose-response, 2b) exposure assessment, and 3) risk characterization [4]. Dose-response assessment can be performed using simulations, but the methods need improvement before they reach the accuracy of laboratory work,

either from field studies or planned laboratory exposure tests. In the latter, one or several chosen model organisms are usually exposed to a range of concentrations, to assess at what concentrations adverse effects can be observed. Common endpoints to be investigated include death, impaired growth or reproduction, or cellular damage such as DNA mutations.

A simple and widely used method to compare the toxic effect between different compounds and organisms is the effect concentration. The effect concentration 50 % (EC50) is the most commonly calculated concentration, and defines the concentration where 50 % of the test population experienced the assessed effect (*e.g.* lowered reproduction). Similarly, the lethal concentration 50 % (LD50) defines the concentration where 50 % of the test population died from the exposure.

When planning dose-response assessment of NPs, special thought must be put into the choice of exposure medium. Toxicity tests on *C. elegans* are commonly performed on agar, in nematode growth medium (NGM), in M9 buffer or in K-medium, but these have been shown to cause agglomeration of NPs and lowered toxicity [25]. To prevent agglomeration, the NPs must be stabilized by steric or electrostatic repulsion. Charged NPs repel each other in a suspension due to Coulomb forces. If the ionic strength (IS) of the medium is high, many free ions are available to screen the repulsion between the particles, and they will more easily agglomerate [26]. To avoid this, a low IS medium can be used. One such recommended medium is moderately hard reconstituted water (MHRW), with a pH of $7.4 - 7.8$, hardness of $80 - 100$ (mg/L $CaCO_3$) and alkalinity of $57 - 64$ (mg/L $CaCO_3$). Another recommended medium with higher ecological relevance is simulated soil pore water [25]. To further stabilize the NPs in the exposure medium, a small fraction of the stabilizing agent Tween 20 can be added. Tween 20 is a non-toxic, non-ionic surfactant, shown to aid in suspension stability and decrease agglomeration of some NPs by steric stabilization [27].

Characterization of ENMs can be done using a wide range of techniques, to determine properties such as size, shape, surface area and charge. For pristine particles and particles in simple aqueous media, there are several useful and acknowledged techniques to measure these properties. Common techniques include electron microscopy such as transmission electron microscopy (TEM) and scanning electron microscopy, atomic force microscopy, dynamic light scattering, nanoparticle tracking analysis (NTA), field flow fractionation, X-ray diffraction and inductively coupled plasma mass spectrometry (ICP-MS) [28, 29]. However, characterization of NP properties and behavior in complex liquid media, soil or living organisms is more challenging. A combination of techniques is often required, while the number of available techniques is often more limited when used in complex biological matrices.

## 2.2 Reactive oxygen species and oxidative stress

In eukaryotic cells, the partial reduction of $O_2$ lead to a continuous production of reactive oxygen species (ROS). Unless neutralized, ROS cause damage

to biomolecules such as proteins, lipids and nucleic acids. The cells effectively remove ROS by enzymes and antioxidants, and under normal conditions the rates of production and removal of ROS are balanced. Environmental stressors such as ionizing radiation or pollutants may increase the production of ROS, causing saturation of enzymes or lack of antioxidants, thereby distorting the cellular redox balance and causing oxidative stress [30, 31].

Important enzymes of the ROS defense system include superoxide dismutase (SOD), glutathione peroxidase (GPX), glutathione s-transferase (GST) and catalase (CAT). Important antioxidants include flavonoids, ascorbic acid, vitamin E and glutathione (GSH). An important ROS is the superoxide anion ($O_2^-$). In the cells, $O_2^-$ is reduced by SOD to $H_2O_2$ which is turned into $H_2O$ and $O_2$ by CAT and GPX (see equations (1) and (2)) [32, 33].

$$2O_2^- + 2H^+ \longrightarrow H_2O_2 + O_2 \tag{1}$$

$$2H_2O_2 \longrightarrow 2H_2O + O_2 \tag{2}$$
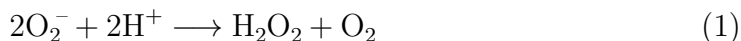
Different SOD enzymes use different metals as cofactors. *C. elegans* have 5 SOD enzymes. SOD-1, SOD-4 and SOD-5 are Cu/Zn isoforms; SOD-1 and SOD-5 are present in the cytosol and SOD-4 in the extracellular matrix. SOD-2 and SOD-3 are Mn isoforms and are found in the mitochondria [34–37]. When the enzymes GST and GSH reduce ROS, GSH can act as an electron donor. This leads to the oxidation of GSH to its oxidized form glutathione disulfide (GSSG) [33].

## 2.3   Cerium oxide nanoparticles

Cerium oxide exists in two forms, cerium (III) oxide ($Ce_2O_3$) and cerium (IV) oxide ($CeO_2$), with the former oxidizing with some rate to the latter. In the following, cerium oxide will refer to cerium (IV) oxide. Cerium oxide is normally found in a cubic fluorite crystal structure. $CeO_2$ NPs are in literature also referred to as ceria NPs or nanoceria. The surface of $CeO_2$ NPs has been reported to contain a substantial number of oxygen vacancies, which leaves electrons with the ability to reduce $Ce^{4+}$ to $Ce^{3+}$ [38]. Shi *et al.* reported that for a sample of $CeO_2$ NPs with a diameter of 3 nm, 18% of the cerium was found as $Ce^{3+}$ [39]. The proportion of $Ce^{3+}$ seem to be strongly dependent on the production method in addition to NP size [40].

Cerium oxide NPs are widely used in applications such as fuel additives, catalytic converters, and chemical and mechanical planarization media [6]. One of the main applications is as a diesel additive where it acts as a catalyst to trap particulate matter, and $CeO_2$ NPs have been detected in the exhaust fumes from diesel vehicles [8, 9]. While reviewing the release, fate and toxic effects of cerium oxide NPs, Collin *et al.* noted that while there is an increasing access to dose-response assessments of $CeO_2$ NPs, there is a lack of exposure assessment.

They stated that estimating the release from other sources than diesel exhaust is currently challenging [6].

A few attempts have been done to perform exposure assessment of $CeO_2$ NPs. Giese *et al.* modelled the concentration of $CeO_2$ NPs in freshwater from 1950 to 2050, and estimated the concentrations to be 1 pg/L in 2017, rising to a few hundred ng/L in 2050 [41]. They concluded that the toxic risk is generally low, but that the increased concentration close to point sources can be of concern.

Johnson *et al.* looked at the concentration of $CeO_2$ NPs in soil in the United Kingdom, caused by their use as a fuel additive and neglecting other sources. Based on commercial information, they modelled the soil concentration within different dispersion scenarios. In the scenario where the particles only dispersed within 20 m from the road, the highest predicted concentration of cerium after seven years of exposure was 16 µg/kg, rising to 40 µg/kg after five years with twice the exposure [42].

A concentration of 16 µg/kg is equivalent to 0.027% of the natural background of cerium, indicating a low risk to organisms. However, the unique properties of nanoparticles and their possibility to induce adverse biological effects at low concentrations cannot be overlooked. The highest estimated concentration of cerium in river water by Johnson *et al.* was 300 ng/L, the same concentration estimated to be found in 2050 by Giese *et al.* [41, 42], illustrating the large uncertainty in exposure estimates. To follow the precautionary principle, one should assume that the highest estimates of exposure and the lowest estimates of effect concentrations are closest to the truth.

## 2.4   Cerium toxicity

Cerium ions have been found to be toxic to a variety of organisms, and several possible mechanisms have been investigated or hypothesized. General cytotoxicity of $Ce^{3+}$ was demonstrated by Lizon and Fritsch, who reported increased fractions of apoptotic cells among rat alveolar macrophages [43]. Paoli *et al.* suggested that the toxicity to the lichen *Xanthoria parietina* was caused by inhibition of enzymes by the binding of cerium ions to functional groups, causing interference with the catalytic action or structural integrity of the enzyme. They also observed extra- and intra-cellular bioaccumulation [44]. In *Arabidopsis thaliana* seedlings, $Ce^{3+}$ was shown to hinder nutrient uptake and translocation in the plant [45]. Du *et al.* reported agglomeration of membrane proteins on erythrocytes after exposure to $Ce^{3+}$ [46], while Shivakumar and Nair reported a decrease in protein synthesis in human cardiac myocytes and lung fibroblasts [47].

Cerium ion solubility and bioavailability is affected by *e.g.* pH, concentration, temperature and medium composition, and the exposure medium is therefore important for the toxic potential [48]. Cerium nitrates are water soluble, while cerium carbonates are insoluble [49–51]. Ma *et al.* performed a toxicity test on *Daphnia magna*, and reported very low fractions of filterable forms of cerium at the beginning of the test and even lower at the end, probably due to the forma-

tion of insoluble cerium carbonate complexes. The precipitation of lanthanides such as cerium may lead to an underestimation of the ecotoxicity. Barry *et al.* reported an EC of lanthanum (La) of $43\,\mu g/L$ for *Daphnia magna* when the exposure medium had a low carbonate hardness, while the EC was $1180\,\mu g/L$ in a standard exposure medium [52]. Precipitates of lanthanide carbonates have been considered biologically inert, but they might pose a particle-specific risk analogous to a nano-specific risk [48].

$CeO_2$ NPs have been shown to be inert, releasing a very low fraction of cerium ions into the liquid media when dispersed [24]. Nevertheless, toxic responses induced by $CeO_2$ NPs have been reported in several organisms, indicating a nano-specific MOA. In addition to reports on toxic responses, there is also a significant number of papers reporting the opposite effect, namely the improved biological function after exposure [10, 53]. This contradiction is believed to originate in the redox-potential of the $CeO_2$ NPs. The ability of surface cerium to cycle between the $Ce^{3+}$ and $Ce^{4+}$ state, means that cerium can act as either an electron donor or acceptor depending on the oxidation state [54]. The NPs may function either as a producer or a scavenger of radicals, depending on the specific properties of the NP and their surroundings [55, 56]. For example, $CeO_2$ NP exposure produced significant oxidative stress in human lung cancer cells, as measured by reduced glutathione and $\alpha$-tocopherol levels, leading to lipid peroxidation and cell membrane damage [57]. Illustrating the opposite effect, $CeO_2$ NPs were shown to demonstrate SOD catalytic activity, and reduced oxidant-mediated apoptosis in human breast fibrosarcoma cells (HT-1080) [10].

A few articles report the effect of $CeO_2$ NPs on nematodes. Lahive *et al.* investigated the toxicity of three different types of $CeO_2$ NPs in the size range 5-80 nm in diameter in the earthworm *Eisenia fetida* [56]. None of the exposure groups were affected, as measured by reproduction and survival. However, they discovered increased concentrations of cerium in the animal tissue, and observed cuticle loss from the body wall and some loss of gut epithelium integrity. They concluded that long-term exposure could possibly cause serious effects.

Zhang *et al.* demonstrated that *C. elegans* experienced ROS accumulation and oxidative damage after exposure to $CeO_2$ NPs of around 8.5 nm in diameter. Decreased lifespan was observed at environmentally relevant concentrations, with a 12 % decrease for the lowest tested concentration of 1 mmol/L cerium [58].

Arnold *et al.* reported the inhibited growth of *C. elegans* after exposure to commercially available $CeO_2$ NPs, with the effect being larger for nano-sized $CeO_2$ than for equimolar bulk $CeO_2$ [59]. Experiments on metal and oxidative stress-sensitive transgenic nematode strains gave weak evidence of an oxidative stress or metal sensitivity mechanism. However, they noted that the inhibition of growth could at least partly be explained by the $CeO_2$ NPs agglomerating around *E. coli* added as the food source, or inside the gut tract. They showed that $CeO_2$ NPs were ingested into the gut, but NPs were not detected inside cells.

## 2.5  *C. elegans*

The roundworm *C. elegans* are free-living, *i.e.* non-parasitic, organisms that in nature live in temperate soil. They are mainly hermaphrodites that self-fertilize as each individual produces both sperm and oocytes. The hermaphrodites can also be fertilized by male individuals, which in nature accounts for only 0.05 % of the population [60]. The worms live for around 3 weeks and reproduce after 3 days, with each individual capable of producing over 300 offspring [11]. By feeding them with bacteria and keeping them in the dark, they are easily maintained in large numbers in the lab. The adults are around 1 mm long and transparent, allowing in-vivo imaging. These traits make them an ideal model organism in research, and they have been extensively used since the 1970s when Sidney Brenner suggested their potential [11, 61].

Figure 1 shows the life cycle of a hermaphrodite *C. elegans*. From the released egg, the worm passes through four larval stages (L1-L4) before adulthood, with each transition marked by molting [62]. When an individual reaches the adult stage, it begins to reproduce. Under difficult conditions such as little food, crowding or heat, the L1 larvae can be arrested in a Dauer state. They can remain in this stress-resistant state for a long time, transitioning directly to the L4 stage if conditions improve [63].

The intestine is one of the major organs, responsible for digestion and macro-molecular metabolism. During reproduction, the adult hermaphrodite eat millions of bacteria per day [65]. *C. elegans* have been shown to defecate every second minute, each time expelling around 30-50 % of the intestinal volume [66]. As a result, the potential residency time for toxic compounds is very short, when assuming a low intestinal uptake and accumulation.

*C. elegans* was the first organism to have its complete genome sequenced, and later the complete connectome, the map of all neural connections [67]. The latter task was simplified by the fact that an adult hermaphrodite has only 959 somatic cells, that develop from the embryonic cells in an identical pattern for all individuals [62]. The *C. elegans* genome contains around 20 000 genes, which is similar in size to the human genome [67].

*C. elegans* are a suitable model organism in ecotoxicity research. By using developed laboratory protocols for obtaining age-synchronized cultures of L1 stage larvae, classical toxicological endpoints such as death or impaired reproduction can easily be evaluated for toxic compounds. In addition, several transgenic strains of *C. elegans* have been developed for investigating the mechanisms behind toxic effects.

One such transgenic strain is the GFP labelled GA508 wuls54[pPD95.77 sod-1::GFP, rol-6(su1006)] (SOD-1) reporter strain. 75 % of the total SOD transcription in *C. elegans* is of the isoform SOD-1. In the SOD-1 reporter strain, a gene coding for GFP is fused with the *sod-1* gene. Consequently, the amount of expressed GFP is correlated with the *sod-1* gene expression, and SOD-1 can be used as a reporter of ROS production and oxidative stress [34]. In addition to the GFP protein, the strain has a different moving motion than the wild type.
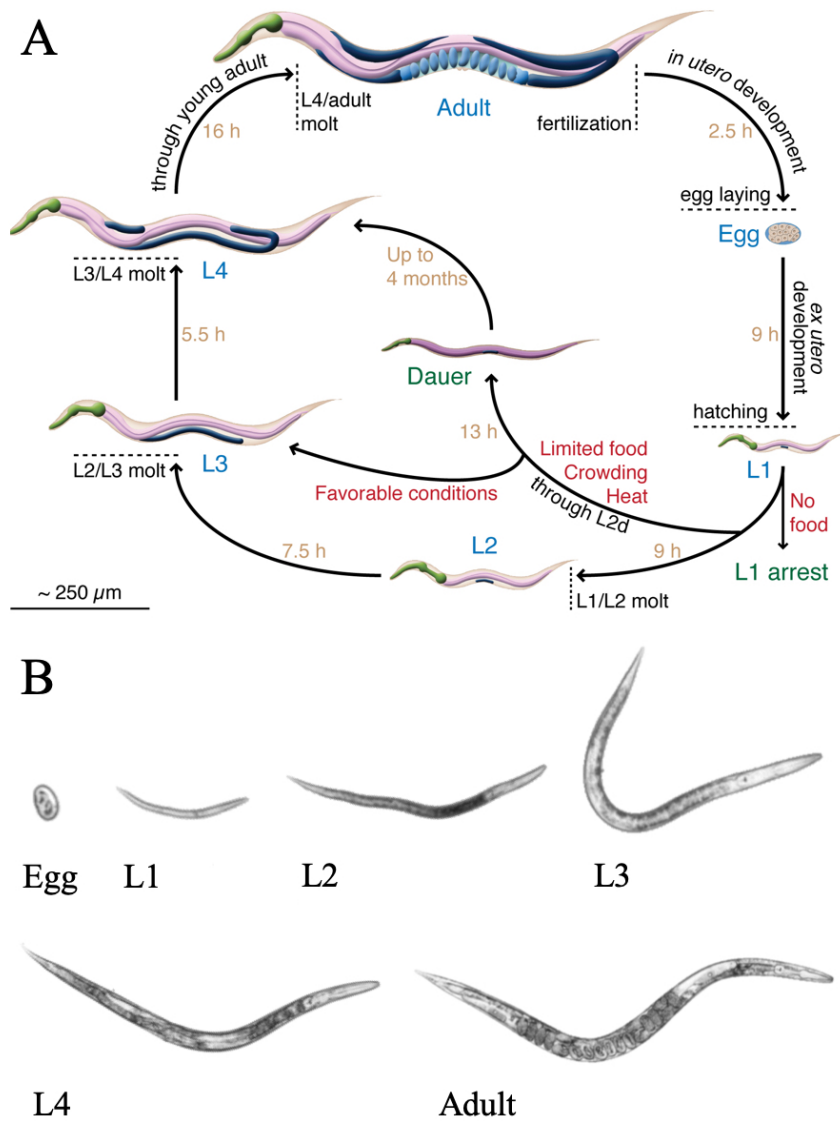
**Figure 1:** Illustration (A) and images (B) of the life cycle of a hermaphrodite *C. elegans*, from eggs via the 4 larval stages to adult. Panel A adapted from [64], images in panel B are taken by the author.

They move by a rolling motion and are called rollers, as opposed to non-rollers such as the wild type. The rollers have a disadvantage as the moving motion is less efficient, and the nematodes are slower in finding food. Due to homologous recombination, some non-rollers will occur after cultivation over several generations. These will also have lost their GFP-producing gene, and thus, to use the strain, the culture needs to be maintained by selecting rollers.

Another transgenic strain developed to investigate the oxidative state is the biosensor strain Grx1-roGFP2 (GRX). The reduction–oxidation-sensitive green fluorescent protein (roGFP) works as a redox-sensitive probe, allowing real time, *in vivo* measurement of the ratio between the oxidized (GSSG) and reduced (GSH) form of the antioxidant glutathione [35]. Glutathione functions as an electron donor during the transformation of peroxides into $H_2O$ and $O_2$, and is present in high concentrations in the cells. Upon a shift in the redox balance in the cell caused by increased ROS concentrations, the ratio of oxidized over reduced glutathione will increase. When GSH is oxidized to GSSG, it leads to a small conformational change in the GFP. This conformational change leads to a small shift in the emitted wavelength when illuminated, and the ratio of oxidized over reduced glutathione can be quantified. Therefore, GRX works as a biosensor of the cellular redox state [68].

The fluorescence emission from GRX is quantifiable, as the measurement is a ratio of the oxidized and reduced form of a molecule. The fluorescence emission from SOD-1 is a quasi-quantifiable measurement, and is useful only when compared to a control value.

## 2.6 Optical microscopy

### Stereo microscopy

Stereo microscopes, also known as stereoscopic or dissecting microscopes, are simple light microscopes used for low magnification imaging. The microscope contains two separate optical paths between the specimen and eyepieces, and the human brain combines the two different paths to a three-dimensional image [69]. The distance between the specimen and objective lens is commonly large enough to *e.g.* pick single nematodes, making it a useful tool in *C. elegans* cultivation and research.

### Phase-contrast microscopy

Using bright-field microscopy, transparent objects such as cells are almost invisible due to the low contrast. Such objects can be imaged by staining, but this requires time-consuming sample preparation, can induce artifacts, and cannot be done on living specimens. To image transparent, living samples, one can instead use phase contrast microscopy. Although most transparent biological specimens do not absorb light, they diffract light, causing a phase shift in the light waves.

This is not visible to the human eye directly, but is exploited in phase-contrast microscopes which translate the phase shift into contrast [69].

**Fluorescence microscopy**

In the last decades, fluorescence microscopy has become an essential tool in biology research. Due to the exceptional contrast and the plethora of available fluorescent probes and transgenic strains, the researcher can visualize different cellular or sub-cellular components in the same specimen.

When fluorescent molecules are illuminated, the incoming photons cause electrons to be excited to a higher energy level. This energy state is unstable, and after a few nanoseconds the electron is returned to the ground state, releasing the energy as a photon with a lower energy and thus longer wavelength [70]. The difference in wavelength between the absorbed and emitted light is called the Stoke's shift, and the bigger the shift the easier it is to distinguish the wavelength peaks for incoming and outgoing light. By filtering out the incoming light and only letting the emitted light pass, only the fluorescent objects are imaged.

Fluorescence microscopes come in simple forms such as epifluorescence microscopes, and more advanced setups such as confocal scanning laser microscopes. Epifluorescence microscopes are similar to standard optical microscopes, with a few adjustments. One is the high intensity light source, commonly a xenon or mercury lamp or a laser. The other is the addition of specialized filters and a dichroic mirror that filter the wanted wavelengths. Figure 2 shows a schematic illustration of the setup. The high intensity light is passed through an excitation filter, and the desired wavelengths are directed to the specimen via a dichroic mirror and the objective lens. The photons excite electrons in the fluorescent molecules in the specimen, and the emitted light passes the objective lens. The light then passes the dichroic mirror and an emission filter, to stop undesired wavelengths from passing to the ocular or digital detector [71]. The two filters and the dichroic mirror are often assembled in a so-called filter cube that can be easily changed by the operator. Different fluorescent molecules can thus be imaged in a specimen, *e.g.* to quantify the ratio between different molecules in a cell.

In theory, the electrons can cycle between the ground and excited states for an unlimited time. However, the chemical conditions often limit the number of cycles to around 10 000 - 40 000 cycles for good fluorophores [70]. This phenomenon is known as photobleaching, and operators should attempt to slow down the process, *e.g.* by avoiding unnecessary exposure of the sample to light. The molecular mechanisms behind photobleaching are not fully known, but is thought to originate from the accumulation of free radicals caused by absorption of the photons, and the following chemical damage to the fluorescent molecules [73].

Molecules that are used because of their fluorescent properties are called fluorophores. Many organic substances are autofluorescent, and some of these can be used to label components of interest. More often, synthesized compounds are used as this allows for optimization of the excitation and emission wavelength
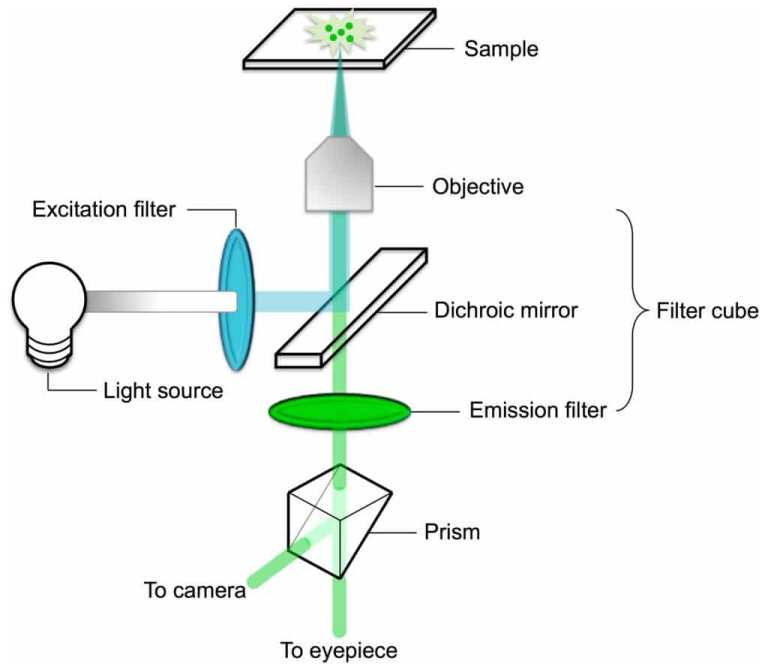
**Figure 2:** The working principle of an epifluorescence microscope. Adapted from [72].

and the efficiency of the fluorophore. In addition, researchers have introduced the use of genetically encoded fluorescent probes, known as reporter genes. The green fluorescent protein (GFP) is the most frequently used reporter gene, and is widely used to genetically tag protein components of living systems. The GFP genes were first cloned from jellyfish in 1992 [74]. Two years later, Chalfie and colleagues showed that the expression of the gene in *C. elegans* led to fluorescence [75]. Most GFPs variants are relatively resistant to photobleaching [76].

## 2.7   Transmission electron microscopy

Transmission electron microscopy is the electron microscopy analogue of light microscopy, using electrons instead of photons to image the sample. The resolution of light microscopy is limited by the wavelength of the incoming light by Rayleigh's criterion. To obtain images with a higher resolution, in TEM one exploits the wave-particle duality of electrons [77]. Electrons have a wavelength inversely proportional to their velocity, given by the de Broglie wavelength $\lambda$:

$$\lambda = \frac{h}{mv}, \tag{3}$$

where $h$ is Planck's constant, $m$ is the mass and $v$ is the velocity. Using high-velocity electrons, the resolution limit of today's TEMs is on the sub-atomic scale [77].

A TEM instrument consists of an electron gun, a lens system, a sample holder and an imaging system. The electron gun has a tungsten filament as cathode,

which releases electrons when heated. The free electrons are accelerated towards the anode and into the lens system. Magnetic lenses focus the electron beam towards the sample holder, and filters the electrons so that the beam consists of electrons in a narrow energy range. The electrons pass through the thin specimen mounted on a conducting grid. Depending on the material, the thickness of the specimen should be in the range of a few nanometers to a few hundred nanometers. The transmitted electrons are collected on a fluorescent screen or a charge-coupled device camera, producing the image of the sample [28].

Limitations include the limited sampling size, a necessary consequence of all high-resolution techniques. Additional techniques should be used to avoid erroneous extrapolation of the data from a few imaged areas to the whole sample, when that may not be correct. Further, 3D objects are projected as 2D images, potentially hiding important information regarding shape. The contrast of TEM micrographs is dependent on both the thickness and the electron density of the specimen at any given point, and they lack depth sensitivity as the information is an average of the thickness of the specimen. Thus, the micrographs contain no information about the potential difference between the surface and bulk of the sample. The electron beam can damage the specimen, and for high-intensity beams or fragile specimens this can lead to artifacts. For liquid NP suspensions, agglomeration of NPs may occur during preparation of the grids due to drying effects. Knowledge of these effects is imperative when interpreting TEM micrographs [77].

The evaluation of the size distribution of non-spherical NPs is challenging. Several options exist for the estimation of NP size, and in this thesis the maximum Feret diameter is used. The Feret diameter is the perpendicular distance between parallel tangents touching opposite sides of the particle perimeter [78]. The maximum Feret diameter is shown in figure 3.
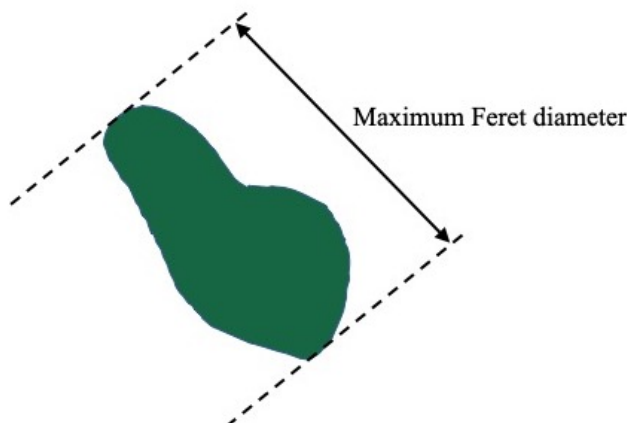


**Figure 3:** The maximum Feret diameter. Illustration by the author.

## 2.8 Zeta potential measurements

Charged particles in an ion solution attract ions with opposite charge due to Coulomb forces. The ions will accumulate at the surface of the particle and form an electrical double layer, see figure 4. The double layer consists of the inner Stern layer where the ions are strongly bound to the surface of the particle, and the outer diffuse layer where they are more loosely bound. Within the diffuse layer there is a boundary called the slipping plane. Ions within this boundary have a large occupancy time close to the surface of the particle, and will travel with it when the particle moves. The zeta potential is defined as the electrical potential at the slipping plane.

The electrical potential determines the stability of the suspension. A large potential of the same sign means the particles will repel each other, and the probability of agglomeration will be lower than for particles with a lower potential. Different limits are used to classify a sample as either stable or unstable, commonly this limit is set to $\pm\,30\,\mathrm{mV}$.
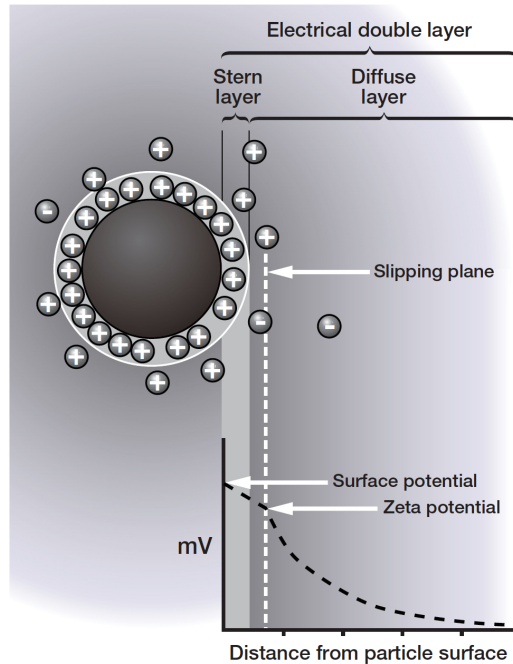
**Figure 4:** Illustration of the electrical double layer of a charged particle in an ion solution. Adapted from [79].

Charged particles move in the presence of an electric field, so-called electrophoresis. The velocity of the particles is called the electrophoretic mobility ($U_E$), and is given by Henry's equation:

$$U_E = \frac{2\epsilon Z}{3\eta} f(\kappa R), \tag{4}$$

where $\epsilon$ is the dielectric constant, $Z$ is the zeta potential, $\eta$ is the viscosity of the

medium, $\kappa$ is the Debye length which represents the thickness of the electrical double layer, and $R$ is the particle radius. $f(\kappa\alpha)$ is called Henry's function. For particles larger than around $200\,\text{nm}$ in a solution with an IS above $1\,\text{mM}$, Henry's function is commonly approximated with the value 1.5, and is then referred to as the Smoluchowski approximation. For smaller particles in solutions with lower salt concentrations, the value of $f(\kappa\alpha)$ is often approximated to 1.0, and Henry's equation is then referred to as the Hückel approximation.

Using equation (4), the zeta potential can be found by measuring the electrophoretic mobility $U_E$. This can be done by applying an electrical field to the sample by using an electrode on each side of the sample. Charged particles will move towards the electrode with opposite charge, and the velocity can be measured. One way to measure the velocity is by laser doppler velocimetry. Laser light is passed through the sample, and the beam at a scattering angle is combined with a reference beam. The resulting laser signal varies in intensity, and the intensity is proportional to the velocity of the particles. To obtain the sign of the zeta potential, one of the laser beams can be modulated using an oscillating mirror. A possible setup of electrophoretic mobility measurements can be seen in figure 5.
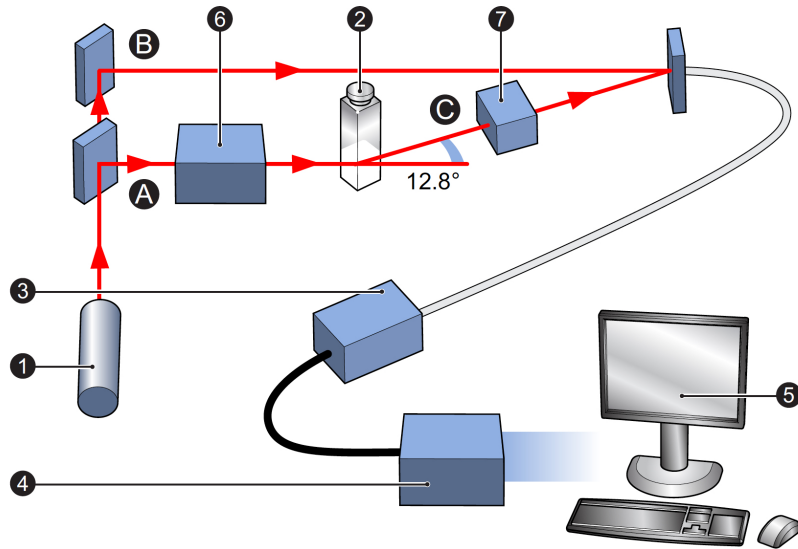


**Figure 5:** Illustrations of the working principle of electrophoretic mobility measurements, used to calculate zeta potential. The laser (1) beam is split into an incident (A) and reference (B) beam. The incident beam is sent via an attenuator (6) through the sample (2). The beam at a scattering angle (C) is sent through compensation optics (7) before reaching the detector (3). The intensity is translated into an electrical signal in a digital signal processor (4), before it reaches the computer (5). Adapted from [79].

## 2.9 Nanoparticle tracking analysis

Nanoparticle tracking analysis (NTA) is a technique used to measure the size distribution of NPs. Unlike techniques such as dynamic light scattering, it is well suited for samples that are non-uniform in size and can provide useful information on the presence of agglomerates and contaminations such as dust. NTA is based on a conventional optical microscope, with a laser light source and a specialized sample holder. A NP suspension is introduced into the sample holder, and the NPs are illuminated using the laser, see figure 6. NPs in aqueous suspension move due to Brownian motion, and the velocity is dependent on the NP size. The NPs are visualized as individual point-scatterers, and the movement is captured by recording videos. Software is then used to analyze the tracks and find the translational diffusion coefficient for the individual NPs [80]. From the translational diffusion coefficient, the sphere equivalent hydrodynamic diameter $d_H$ can be calculated by applying the Stokes-Einstein equation:

$$d_H = \frac{kT}{3\pi\eta D} \tag{5}$$

where $k$ is the Boltzmann constant, $T$ is the temperature, $\eta$ is the viscosity of the medium and $D$ is the translational diffusion coefficient.
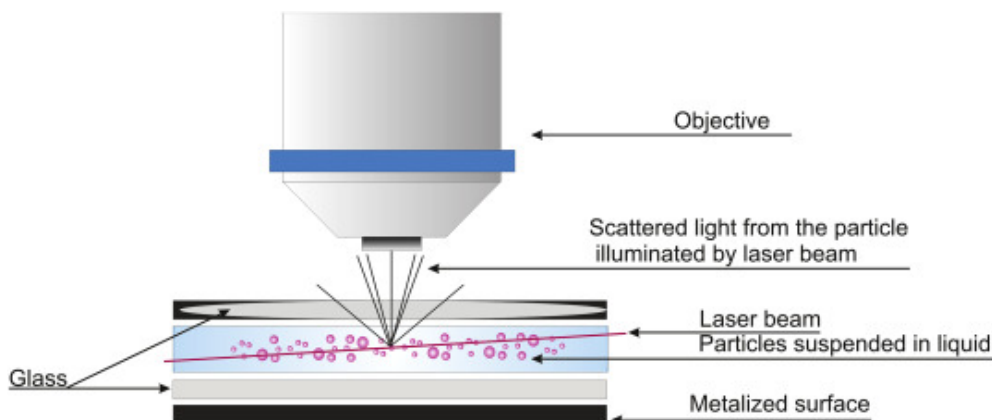


**Figure 6:** Illustration of the working principle of NTA. Adapted from [81].

## 2.10 Inductively coupled plasma mass spectrometry

An inductively coupled plasma mass spectrometer (ICP–MS) is a mass spectrometer that uses high temperature plasma for ionization [82]. The high sensitivity of the instrument makes it a powerful tool for detecting trace elements or determine concentrations in dilute samples [83]. It has a large linear dynamic range and the capability of measuring many elements simultaneously. This has made ICP-MS the most widely used method for determining metal concentrations, ideal for characterizing metal-based ENMs [84, 85]. It can also be used to analyze single

NPs, with the possibility of measuring size distribution, impurities, dissolution rates *etc.* [85].

Figure 7 illustrate the working principle of the instrument. Liquid samples are often mixed with dilute nitric acid before sampling. The sampled liquid is converted into an aerosol by a nebulizer before entering the argon plasma. The free electrons in the plasma ionizes the atoms in the sample, and the resulting positive ions enter into one or several quadrupole mass analyzers. Here, the ions are separated by their mass over charge ratio, and ideally only analyte elements will travel in a stable path and reach the mass detector. The detected signals are compared to a calibration curve, created from the results from standard solutions with known concentrations. The standard solutions are commonly prepared from certified standards, to ensure accurate concentrations and minimal contamination [84]. The sample concentrations need to be low to avoid clogging of the instrument or excessive damage to the detector, and sample dilution is an important step in sample preparations for concentrated samples [85].
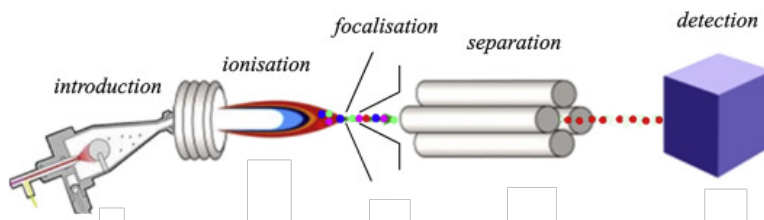


**Figure 7:** Illustration of the working principle of ICP-MS. Adapted from [86].

The major drawback to the technique is different types of interference, mainly the isobaric, polyatomic and matrix effects. Isobaric interference is due to the similar mass of isotopes from different elements, causing a signal from an isotope of a different element to be confused with the analyte isotope. This can be avoided by measuring another isotope of the analyte element, and calculate the concentration of the analyte isotope of interest based on the natural ratio of the analyte isotopes.

Polyatomic ions arise in the plasma when two or more atoms combine. If the combined mass over charge ratio is similar to one of the analytes, the resolution will determine if the two signals can be separated. To avoid a signal from polyatomic ions, some set-ups include the introduction of helium gas into the instrument after ionization. Polyatomic ions have a large diameter compared to the monoatomic analyte, and will collide more frequently with the helium molecules. The ion beam is then filtered based on the kinetic energy of the ions, and the polyatomic ions will not pass.

Matrix effects can cause unwanted signal enhancement or suppression [83]. To minimize this effect, an internal standard is often used. The internal standard is prepared from a certified reference material of an element not present in the sample. A fixed volume of the internal standard is added to all samples before the aerosol is created. The ratio of the analyte concentration over the internal standard concentration will remain constant, and is used to correct the results.

# 3 Materials and methods

## 3.1 Nanoparticle suspension

A stock suspension was prepared of $CeO_2$ NPs (544841, Sigma Aldrich). About 10 mg $CeO_2$ NPs was added into a 15 ml Falcon tube in a fume hood. The exact weight was measured before adding double-distilled water ($ddH_2O$) with 0.2 % Tween 20 (P1379, Sigma-Aldrich) to a NP concentration of 1 mg/mL. The suspension was vortexed at 3000 rotations/min (MS3 basic, IKA) for 5 minutes, before being alternately sonicated at 35 kHz (Sonorex RK106, Bandelin) for 5 minutes and vortexed for 10 seconds for 1 hour.

Three replicate stock suspensions were created by diluting 1 mL of the NP suspension $10\times$ in moderately hard reconstituted water (0.44 mM $CaSO_4$, 0.50 mM $MgSO_4$ and 1.14 mM $NaHCO_3$, adjusted with $HNO_3$ to pH 7.7) with 0.2 % Tween 20 (MHRW T). The stock suspensions were again alternately sonicated for 5 minutes and vortexed for 10 seconds for 1 hour.

The stock suspensions were left for 24 hours without agitation, to allow for sedimentation of NP agglomerates. Large agglomerates are assumed to have no effect on the toxicity and were excluded at this stage for a more accurate characterization of the available cerium concentration. After 24 hours, aliquots were pipetted out from the 5 mL mark, and immediately used for toxicity testing or characterization.

The final concentration of cerium in the pipetted aliquots was estimated to be less than the initial concentration, due to the observed sedimentation in the diluted stock suspensions after 24 hours. Based on results from the project thesis, the concentration in the aliquots was assumed to be 80 % of the initial concentration. Throughout this thesis, all cerium concentrations in the NP suspensions are calculated from this assumption.

## 3.2 Characterization of nanoparticle size distribution

Two methods were used to assess the size distribution; TEM and NTA. During the project work, TEM micrographs were taken of the $CeO_2$ NPs in MHRW T, ethanol and $ddH_2O$ (see appendix B). The micrographs of $CeO_2$ NPs in $ddH_2O$ had high contrast, and the NPs were seen to be well separated with a low degree of agglomeration. These micrographs were used throughout the master work to assess the size distribution, using the image analysis software ImageJ.

The micrographs were obtained during the project work as follows: A suspension of $CeO_2$ NPs in $ddH_2O$ was prepared following the protocol in section 3.1, but using $ddH_2O$ as solvent in all steps. From the prepared suspension, a 5-10 µL drop was pipetted onto a Pioloform coated 400 mesh copper grid (AGS134-4, Agar Scientific). The grids were left to air-dry, covered by a petri dish to minimize contamination. The samples were imaged within a week, using a TEM Morgagni 268 operating at 80 keV.

The image analysis was performed by manually tracing the edges of the NPs using the polygon selections tool in ImageJ, see figure 8. 300 NPs from 5 micrographs were traced, and the measured maximum Feret diameters used to plot a histogram of the size distribution (see section 4.1).
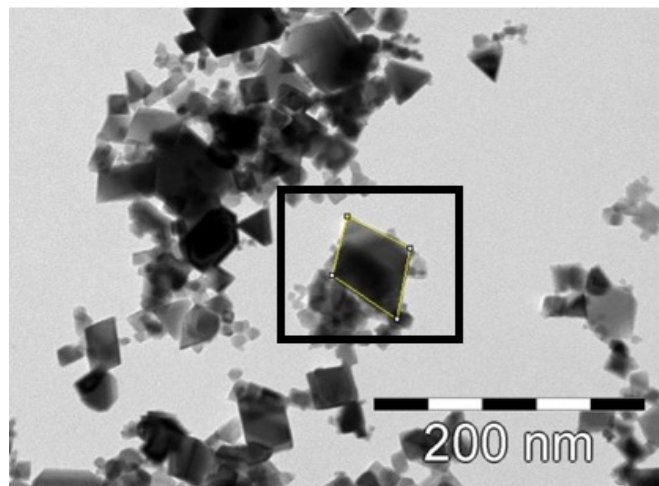


**Figure 8:** Image analysis of the NP size distribution from TEM micrographs. Using image analysis software, the perimeter of each NP was marked manually as seen in yellow in the image, and the maximum Feret diameter measured by the software.

NTA was performed on $CeO_2$ NPs in three different suspension media; $ddH_2O$, MHRW and MHRW T. Stock suspensions were prepared at CERAD (t=$-24$ h). At t=0 h, 1.5 mL suspensions were pipetted from the 5 mL mark into an Eppendorf tube. All samples were transported to NTNU NanoLab (at room temperature), where the NTA was performed at t=120 h. A suitable dilution for optimal measurements was found by trial and error. The results presented here were measured from a sample of stock suspension diluted 1:200 in $ddH_2O$. The Eppendorf tube was shaken vigorously by hand before dilution. The NTA was performed using a Nanosight LM10 (Malvern Panalytical). A blue laser with wavelength 488 nm was used to illuminate the NPs, and 5 videos of 60 seconds were recorded per sample.

The results of the measurements conducted on $CeO_2$ NP suspensions in $ddH_2O$ are presented in section 4.1. The NPs in MHRW had a very low bulk concentration, due to the substantial agglomeration as seen in the bottom of the stock suspension at t=0 h. These samples did not produce good results and are not presented here. For the samples in MHRW T, the author did not manage to inject the samples into the sample holder without the formation of bubbles. As bubbles introduce large errors into the measurements, these results are not presented.

Based on previous knowledge of the size distribution, a manual cut-off diameter of 300 nm was set when plotting the final results.

## 3.3 Characterization of nanoparticle zeta potential

The zeta potential of the NPs was measured by electrophoretic mobility measurements. 1 mL of the prepared NP suspension was added to a folded capillary zeta cell (DTS1070, Malvern Panalytical). The cell was placed in the sample holder of a Zetasizer Nano ZS (Malvern Panalytical), and the measurements run automatically. The folded capillary zeta cell was rinsed before and between measurements with ethanol and ddH$_2$O. The Malvern Zetasizer Software was used to estimate the zeta potential from the electrophoretic mobility, using the Smoluchowski equation and the optical properties listed in table 1.

**Table 1:** Optical properties used for electrophoretic mobility measurements.

| Property | Value | Unit |
|---|---|---|
| Refractive index | 1.59 | |
| Absorption | 0.01 | |
| Viscosity | 0.9308 | cP |
| Temperature | 23 | °C |

## 3.4 *C. elegans* cultivation

The N2 strain was acquired from *Caenorhabditis* Genetic Center, USA, the biosensor strain GRX from the Laboratory for Aging Physiology and Molecular Evolution (University of Ghent, Belgium) and the reporter strain SOD-1 from the Institute of Healthy Aging Genetics, University College London, England.

Liquid nematode cultures were kept alive by performing the protocols described below twice a week. All handling of *Escherichia coli* (*E. coli*) and *C. elegans* was done aseptically, by working in a laminar flow cabinet using sterile equipment. Erlenmeyer flasks, pipette tips and liquid media were autoclaved before use.

**Preparation of growth medium**

*E. coli* OP50 was added to the growth medium as the food source for *C. elegans*. Single cell colonies were grown on a streak plate, by transferring *E. coli* from a liquid stock stored at -80 °C onto a lysogeny broth (LB) agar (0.17 M NaCl, 10 g/L Tryptone, 5 g/L yeast extract and 12 g/L agar) plate using a sterilized inoculation loop. The loop was then used to create a pattern diluting the concentration in each quadrant of the plate. The streak plate was incubated overnight at 37 °C, then stored at 4 °C and used to make liquid *E. coli* cultures for a maximum of two weeks before discarding it.

Liquid *E. coli* culture was prepared by measuring 50 mL LB into a flask, and gently transferring an *E. coli* colony from the streak plate into the flask with a

sterilized inoculation loop. The culture was then incubated overnight at 37 °C with gentle shaking to ensure sufficient oxygenation (200 rotations/min).

The next day the *E. coli* was washed and extracted from the liquid culture before adding it to the growth medium. 50 mL *E. coli* culture was washed by centrifuging at $5000g$ for 5 minutes and removing the supernatant. This was followed by rinsing twice with S-base (51 mM NaCl), using the same centrifuge parameters. The pellet was suspended in 50 mL S-base with cholesterol (51 mM NaCl, 1 mM $CaCl_2$, 1 mM $MgSO_4$, 25 mM $KPO_4$, 0.13 µM cholesterol) at room temperature and transferred to a flask.

### Preparation of *C. elegans* culture

A three to four days old liquid culture of *C. elegans* was checked by light microscopy to ensure healthy and gravid hermaphrodites. Around 500 µL of *C. elegans* culture was then added to 50 mL prepared growth medium. The flask was stored in the dark at 20 °C, with gentle shaking (125 rotations/min). When preparing the final culture for the toxicity tests, the volume of the liquid *C. elegans* culture was adjusted to ensure sufficient L1 stage larvae for the test plates.

### Age synchronization

The liquid *C. elegans* culture was bleached to obtain free eggs for an age synchronized population. 25 mL of the culture was centrifuged at $800g$ for 2 minutes. The supernatant was then carefully removed, leaving the visible cluster of nematodes. The volume was adjusted to 25 mL with S-base, before repeated centrifugation and removal of the supernatant. Next, the volume was adjusted to 7.67 mL with $ddH_2O$.

1.3 mL sodium hypochlorite (425044, Honeywell) and 1 mL NaOH (5 M) was added. The content was continuously mixed by shaking the tube and vigorously suspending and resuspending the content with a pipette. The combined mechanical and chemical stress destroy the nematodes, while the eggs are more resistant due to the protection by the eggshell. After 5 minutes, the nematodes were checked frequently by light microscopy until mostly free eggs were seen, with no or very few intact adults. This lasted for a maximum of 1 minute to avoid damage to the eggs, before the protocol was continued.

The tube was then centrifuged at $1000g$ for 1 minute. The eggs were washed three times by adjusting the volume to 25 mL with M9 buffer (22 mM $KH_2PO_4$, 42 mM $Na_2HPO_4$, 86 mM NaCl, 1 mM $MgSO_4$) and centrifuging at $1000g$ for 2 minutes. In the last round, the supernatant was removed until around 3.5 mL remained, before resuspending the cluster of eggs in the remaining liquid. The liquid was added to a nematode growth medium (51 mM NaCl, 1 mM $CaCl_2$, 1 mM $MgSO_4$, 25 mM $KPO_4$, 13 µM cholesterol, 17 g/L agar, 2.5 g/L peptone, NGM) plate, and stored in the dark overnight at 20 °C with gentle shaking (75 rotations/min). The lack of food ensures that the hatched larvae stay in the

same developmental stage, even though individual eggs hatch at slightly different times.

## 3.5   Liquid medium effect on nematode growth

MHRW was used as the toxicity suspension in all tests, and does not contain cholesterol. During nematode cultivation between toxicity tests, cholesterol is added to the growth medium (S-base) as described by the protocols above. Cholesterol is necessary to ensure normal nematode development over the course of several generations. In multi-generational studies, cholesterol must be added to the toxicity medium. For single generational studies, the procedures vary between researchers.

To inspect the effect of the presence or lack of cholesterol in the toxicity suspension, a synchronized culture of GRX was left for 72 h in three different media; MHRW, MHRW with cholesterol, and S base with cholesterol. The test setup was the same as for the toxicity tests described in section 3.6, but no cerium was added.

## 3.6   Toxicity tests

### Experimental overview

Two toxicity tests were performed for each nematode strain during this work, due to challenges during the first attempt. The results from the last test of each nematode strain are presented in sections 4.3 and 4.4. See table 2 for details, including a brief comment on the experienced challenges. The challenges for E2 in are discussed in section 5.1, and for E4 and E5 in section 5.3.

**Table 2:** Performed toxicity tests.

| Test | Strain | Challenges | Results presented |
|------|--------|------------|-------------------|
| E1* | N2 | | No |
| E2 | N2 | Dose-response deviating from E1 | Yes[a] |
| E3 | N2 | | Yes |
| E4 | SOD-1 | Too few nematodes | No |
| E5 | SOD-1 | Nematode culture issues | Yes |
| E6 | GRX | Microscope software problems | No |
| E7 | GRX | Microscope software problems | Yes[b] |

*E1 was performed during the project work, and is listed for comparison with E2 and E3 in this thesis.
[a] Only ICP-MS results, found in appendix C.
[b] Complete results, except for $33\,mg/L$ cerium from $CeO_2$ NP exposure at t=72 h.

## Procedure

The toxicity tests were carried out as 96 h (N2) or 72 h (SOD-1 and GRX) chronic toxicity tests. The test is based on the International Organization for Standardization (ISO) 10872:2010 standard for water quality, with some modifications [87]. Mainly, the test medium was changed to MHRW, as it is better suited to study NP toxicity as discussed in section 2.1. The nematodes were exposed to $Ce^{3+}$ or $CeO_2$ NPs in sterile 24 well cell culture plates, see figure 9 for an illustration of the test setup.

$CeO_2$ NPs were tested in the range 0.51 to 33 mg/L of cerium, with seven concentrations in the N2 toxicity test and three concentrations in the SOD-1 and GRX tests. The ion solution was tested in 12 concentrations ranging from 2 to 26 mg/L cerium in the N2 toxicity test, and three concentrations in the range 0.32 to 11 mg/L cerium in the SOD-1 toxicity test and 2 to 10 mg/L cerium in the GRX tests.

The prepared NP stock suspensions contained NPs in MHRW T with 10 % ddH$_2$O (MHRW T 90), see section 3.1. To make conditions equal for all samples, all diluted NP suspensions, ion solutions and control solutions were prepared in MHRW T 90. Diluted 1:1 with *E. coli* and *C. elegans* in MHRW T, the final solvent was MHRW T with 5 % ddH$_2$O.

Each concentration was tested in triplicate wells. For $Ce^{3+}$, one stock solution was used to make all dilutions. For the $CeO_2$ NPs, three replicate stock suspensions from the same initial suspension were used, as described in section 3.1. The control was performed in three replicates per plate. Controls contained the same volume of *C. elegans* and *E. coli* as test wells, with the remaining volume being MHRW T 90 instead of ion solution or NP suspension.

*E. coli* for the test plates was prepared according to the protocol described in section 3.4, with some adjustments. The washing steps of the liquid *E. coli* culture were done first in MHRW, then in MHRW T, and the pellet was dissolved in MHRW T. The final volume of the culture was halved, to obtain the correct final concentration of *E. coli* in the test wells.

The dilutions of the NP suspensions were performed directly in the test plates, as two-fold serial dilutions. 1 mL from the three replicate NP suspensions was added to one of the three wells marked with the highest concentration. All other wells were filled with 500 µL MHRW T 90, including controls. 500 µL was transferred from the highest concentration wells to the second highest concentration wells, and the content mixed well with the pipette. This step was repeated for all concentrations until lastly 500 µL was removed from the lowest concentration wells and disposed of.

For the ion solution, dilutions were prepared from a 10 mM stock solution of Ce(NO$_3$)$_3$ (22350, Honeywell Fluka) in ddH$_2$O. An intermediate solution was prepared by diluting the stock 1:10 in MHRW T, to make the solvent MHRW T 90. Dilutions to twice the final concentrations were made using MHRW T 90. Intermediate dilutions were prepared to minimize uncertainty from pipetting, always keeping three significant digits. The dilutions were prepared in 15 mL

Falcon tubes immediately before use, due to observed absorption to the tube walls with time, believed to be caused by Tween 20.

The agar plates with L1 stage *C. elegans* larvae were checked by optical microscopy to ensure healthy larvae, that all eggs had hatched, and that they were similar in length. The larvae were transferred to a beaker by adding MHRW T to the plate and swirling gently, before transferring the liquid via a pipette. For the N2 toxicity test, the suspension was diluted in MHRW T to a density of $11 \pm 2$ nematodes /20 µL. For the SOD-1 and GRX toxicity tests, the suspension was diluted to a density of *ca.* 50 nematodes /20 µL. 480 µL *E. coli* suspension were added to all wells, including controls. Lastly, 20 µL *C. elegans* suspension were added to all wells, making the total volume in all wells 1 mL. The plates were covered with lids and stored in the dark at 20 °C, with gentle shaking (100 rotations/min). For E2 and E3, duplicate plates were prepared for assessing the cerium concentration using ICP-MS (see section 3.7).

For the N2 toxicity test, the test was terminated by killing the nematodes after 96 h. 500 µL Rose Bengal (616 µM) was added to each well to stain the nematodes for easier analysis. The plates were then heated at 80 °C for 10 minutes and stored at 5 °C until analysis, which was completed within six weeks. For the SOD-1 and GRX toxicity tests, the nematodes were analyzed *in vivo* after 48 and 72 h.



**Figure 9:** Test setup for GRX. Two sets of plates were prepared, one for analysis at t=48 h and one at t=72 h.

### Analysis of the N2 toxicity test

All wells were assessed using a stereo microscope (M205 C, Leica) equipped with a digital camera (MC170 HD, Leica). Growth was determined by measuring the length of the nematodes using the Leica Application Suite software (LAS

v4.9). Fertility was determined by counting the number of gravid nematodes and dividing by the total number of adults in each well. A nematode was considered gravid if it contained at least 1 egg. Reproduction was determined by counting the number of offspring using a hand held tally counter and dividing by the number of adults in each well.

## Analysis of the SOD-1 and GRX toxicity tests

SOD-1 and GRX nematodes were imaged *in vivo* using a fluorescence microscope (Leica DM6 B) with a CCD camera (Leica DMC 4500). Each sample was prepared right before imaging, to avoid stress for the nematodes and following errors in the results. The content of each well was transferred to an Eppendorf tube, and the nematodes left to settle at the bottom. The nematodes were washed once by removing most of the liquid, adding S base and letting the nematodes settle again. 10 µL 30 µM $NaN_3$ was pipetted onto a microscope slide, before pipetting 10 µL from the bottom of the Eppendorf tube. $NaN_3$ immobilizes and straightens the nematodes. The slides were left for a minute to allow the effect to occur, and to minimize the risk of the nematodes bursting due to the pressure from the cover slip. A cover slip was then carefully placed on top of the microscope slide. If a nematode burst during imaging (see figure 11b), a new nematode was imaged and the image with the bursting nematode was excluded from analysis.

Imaging took around 8 hours and the samples were imaged from the highest to the lowest concentration of cerium, to avoid registering an effect caused by stress. All samples were kept in the dark until imaging, but the plates were not stirred for optimal oxygen levels. For the SOD-1 strain, 18 nematodes were imaged from each exposure group. Due to culture challenges, 5-9 nematodes were manually picked for analysis based on the qualitative appearance of the fluorescence. Two outliers were removed after analysis. See section 5.3 for further details and discussion.

For the GRX strain at t=48 h, 19 controls were imaged at the beginning and 23 nematodes at the end of the day, to see if there were any changes in signal during the day. For all other samples, 24 nematodes were imaged at t=48 h and 18 nematodes at t=72 h. At least 4 nematodes were imaged per triplicate.

The nematodes were imaged at 10x, in phase contrast mode to assess the length, and in fluorescence mode to analyze ROS response to the cerium exposure (see figure 10). At t = 48 h, the nematodes were small enough to be imaged in one frame. At t = 72 h, most nematodes were imaged in two frames due to the increased length, see figures 11e and 11f. A few nematodes were paralyzed in a curled position, allowing for one image per nematode (see figure 11d). The number of imaged GRX nematodes were reduced from 24 at t=48 h to 18 at t=72 h, due to the substantial increase in time needed to image one nematode. The xy-position was manually adjusted between the frames to minimize overlapping or missing parts of the nematode. In three images, two full nematodes were present. In these images, both fluorescence signal and size were averaged before further analysis, see figure 11a.
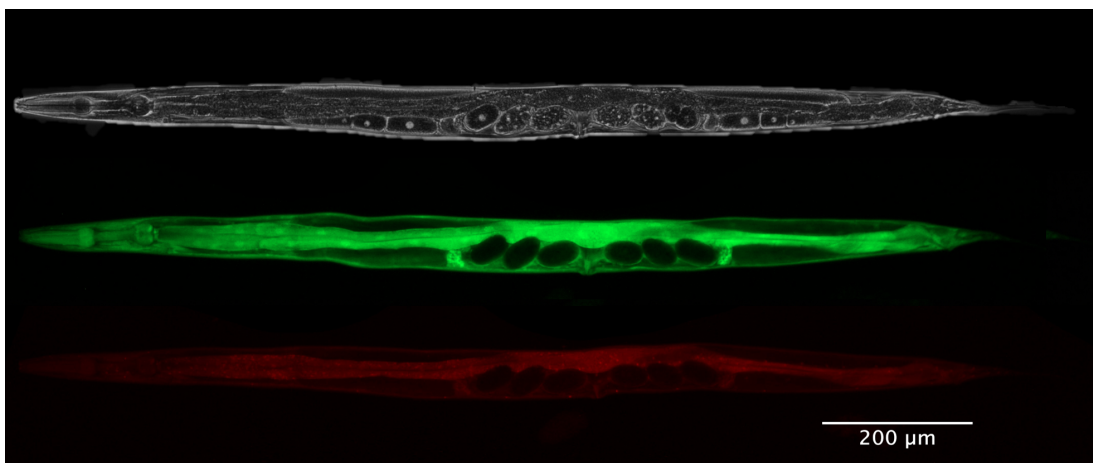
**Figure 10:** Phase contrast (top) and fluorescence (middle and bottom) images of a GRX nematode from the control group at t=72 h. The phase contrast image is used to measure the nematode length, the fluorescence images are used to quantify the fluorescence signal. The nematode is straightened post-imaging using image analysis software.

Fluorescence for SOD-1 and reduced GRX was imaged using a 405 nm excitation and 535 nm emission filter. Oxidized GRX fluorescence was imaged using a 490 nm excitation and 535 nm emission filter. The size of the nematodes was measured using the image analysis software ImageJ, as shown in figure 11c. The fluorescence was quantified using the Leica Application Suit X imaging software and measured by pixel based average intensity. For SOD-1, the average fluorescence signal for each nematode was divided by the size of the same nematode. For GRX, the ratio of signal from oxidized and reduced glutathione was calculated.

Figure 12 illustrates the need to normalize the fluorescence results with the nematode size. In the figure, the top nematode is from the control group, and the bottom nematode from the $11\,\text{mg/L}$ $Ce^{3+}$ exposure group. The reduced growth for the nematode exposed to cerium is easily seen. When measuring one fluorescent protein and not a ratio between two as for GRX, the fluorescence should be divided by the size to account for the different developmental stages.

## 3.7   Characterization of cerium concentration

ICP-MS was performed to assess the cerium concentration in the N2 toxicity tests. Measurements were done on triplicates of a low, medium and high concentration for both $Ce^{3+}$ ions and $CeO_2$ NPs (see table 4 in section 4), plus six samples of the control. Sampling was done at t=0 h and t=96 h, to assess any change in cerium concentration during the course of the test. Possible reasons for a change in concentration include solvent evaporation and binding of cerium to the plastic of the wells.

All samples were acid digested to decompose the cerium into ions. 150 µL from each well was added to Teflon tubes together with $5\,\text{mL}$ Ultrapure $HNO_3$. The
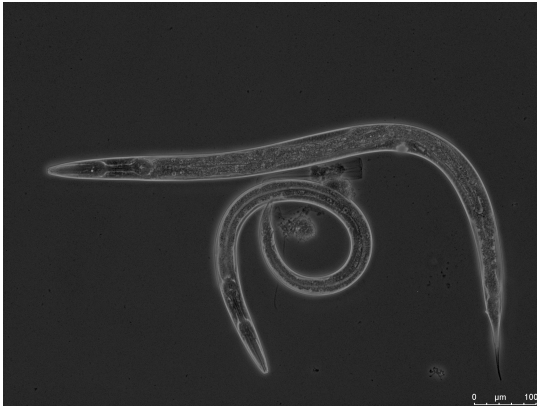
**(a)** Image where fluorescence and length were averaged before analysis.

**(b)** Example of bursting of a nematode during imaging.
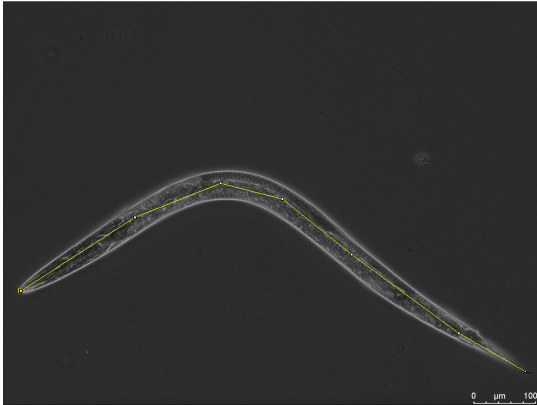
**(c)** Illustrating the measurement of length using ImageJ.
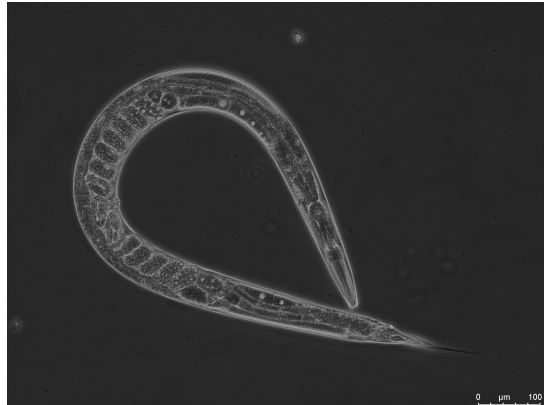
**(d)** Curling of an adult nematode during imaging.
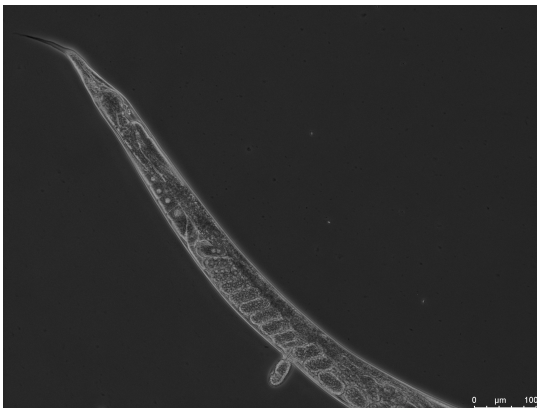
**(e)** Part A of a nematode at t=72 h.
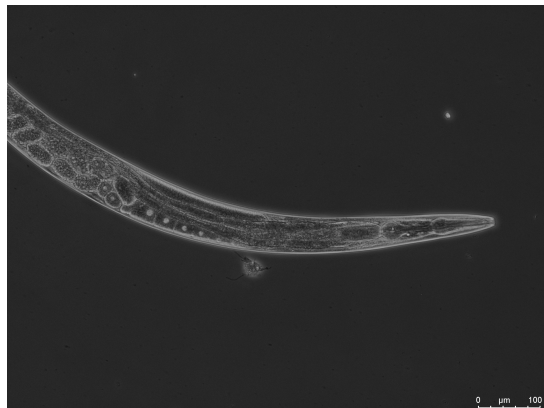
**(f)** Part B of a nematode at t=72 h.

**Figure 11:** Image analysis of SOD-1 and GRX nematodes.

**Figure 12:** Fluorescence images of SOD-1 nematodes at t=72 h from the control group (top) and 11 mg/L Ce$^{3+}$ exposure group (bottom). The nematodes are straightened post-imaging using image analysis software for easier comparison.

tubes were treated in a microwave digestion system (UltraWave, Milestone) at 40 bar, with the temperature rising to 260 °C during 18 minutes and sustaining this temperature for 20 minutes. The samples were then transferred to 50 mL Falcon tubes, rinsing the T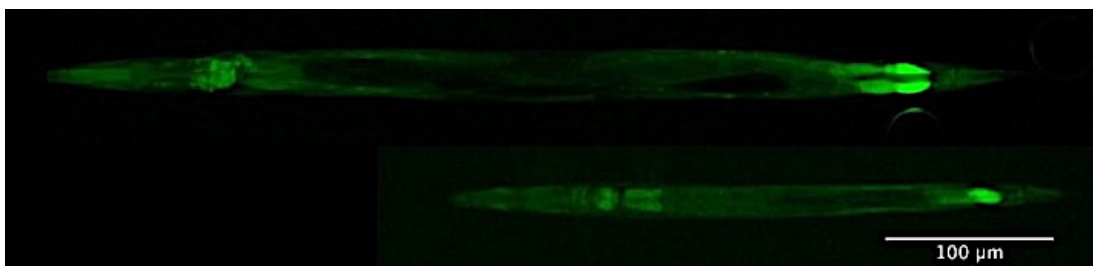eflon tubes three times and diluting the sample to 50 mL with ddH$_2$O. Samples with an estimated cerium concentration above 50 µg/L were further diluted in ddH$_2$O with 10 % Ultrapure HNO$_3$.

The prepared samples were inserted into an autosampler (ASX-500 Series, Agilent Technologies) connected to the ICP-MS (8900 Triple Quad, Agilent Technologies). A calibration curve was created by measuring standard samples of 2 µg/L and 20 µg/L cerium, prepared from a certified standard. All measurements were done in 10 repetitions of 1 second each. The 20 µg/L standard was sampled repeatedly every 10 samples, to permit post-measurement drift corrections. For example calculations, see appendix A.

To assess the degree of sedimentation in the NP suspensions, stock suspensions were analyzed using ICP-MS at different time points. The suspensions were stored without agitation, and samples were pipetted from the 5 mL mark. The first sampling was done immediately after making the suspension at t=-24 h, then at t=0h corresponding to the start of the toxicity test, t=72 h and lastly at t=96 h.

The limits of detection and quantification were set to 3× and 10× the SD of the controls, respectively.

## 3.8 Statistical analysis

Statistical analysis was performed using R 3.5.2 (R Core Team, 2018). Following descriptive statistical analysis, a one-way analysis of variance (ANOVA) was performed to check for statistically significant differences between groups. If this was found, a post-hoc Tukey's Honestly Significant Difference (HSD) test was applied to find the p-values between all group combinations. Differences were considered statistically significant for p<0.05.

# 4  Results

## 4.1  Nanoparticle characterization

TEM micrographs of $CeO_2$ NPs in different media were taken during the project work, see appendix B. In the present work, micrographs of $CeO_2$ NPs in $ddH_2O$ (see figure 13) were used to measure the particle size distribution using image analysis software. The distribution of the maximum Feret diameter is shown in figure 14a. The majority of the particles were measured between 0 and 50 nm, with the peak around 10 nm and a few outliers between 50 and 100 nm.
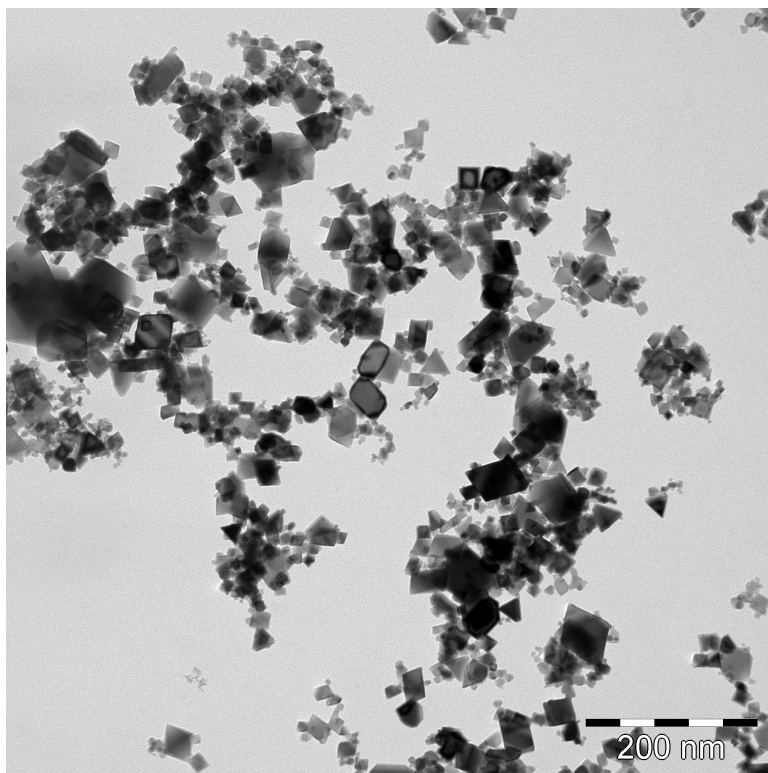


**Figure 13:** Transmission electron microscopy (TEM) micrographs of $CeO_2$ NPs in $ddH_2O$, taken during the project work.

NTA was performed on diluted stock suspensions of $CeO_2$ NPs in $ddH_2O$. The distribution of hydrodynamic diameter can be seen in figure 14b. The majority of particles were measured between 0 and 200 nm, with the peak around 60 nm.

Stock suspensions of $CeO_2$ NPs were measured by electrophoretic mobility measurements to find the zeta potential, see table 3. Two samples were measured for each medium, with the uncertainty not affecting the reported values at two significant digits. Samples in MHRW and MHRW T are similar in value and regarded unstable, while the sample in $ddH_2O$ is higher and considered stable.

To assess the true concentration of cerium during the toxicity test, samples were measured by ICP-MS at the beginning and end of E2 and E3 for a low, medium and high concentration of the $Ce^{3+}$ and $CeO_2$ NP samples. The results
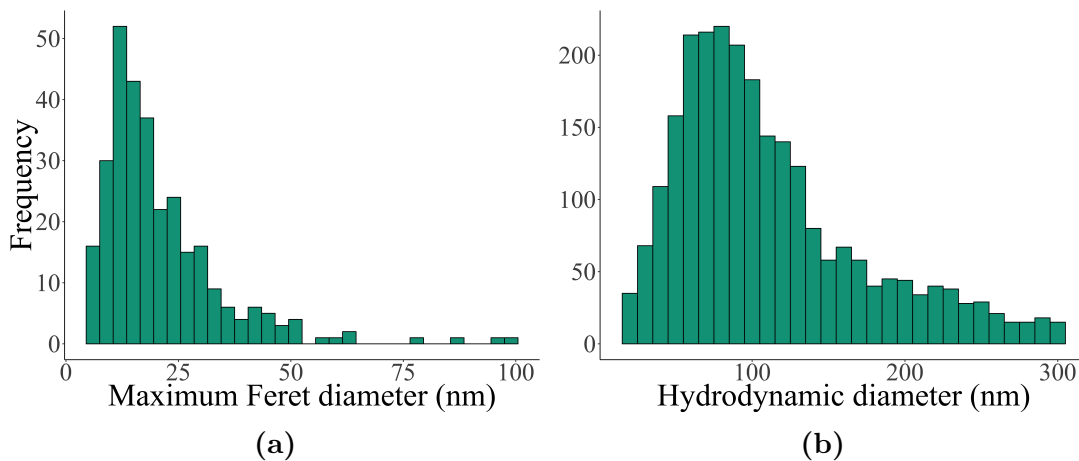
**Figure 14:** Histograms of the size distribution of CeO$_2$ NPs measured using TEM (a) and NTA (b). Note the different range of x-values for the two graphs. The maximum Feret diameters in (a) are measured from N=300 NPs from 5 TEM micrographs. The hydrodynamic diameters in (b) are measured from 5 videos of 60 seconds, and an upper cut-off at 300 nm was set when plotting the results.

**Table 3:** Zeta potential of CeO$_2$ NPs, as measured by electrophoretic mobility measurements. Mean of two samples per medium.

| Suspension medium | Zeta potential (mV) |
|---|---|
| ddH$_2$O | 34 |
| MHRW | $-9.8$ |
| MHRW T | $-10$ |

are summarized in table 4. All samples show a measured concentration close to the expected value at both sampling times, with small variance. For comparison, the ICP-MS results from E2 are listed in table 5 in appendix C.

**Table 4:** Cerium concentration (mean $\pm$ 1 standard deviation) in the exposure media for E3, measured by ICP-MS. N=3, each replicate was measured $10 \times 1$ second.

| Exposure | Estimated concentration (mg/L) | Measured concentration at t=0 h (mg/L) | Measured concentration at t=96 h (mg/L) |
|---|---|---|---|
| $CeO_2$ NPs | 0.59 | $0.47 \pm 0.044$ | $0.52 \pm 0.014$ |
| | 4.7 | $4.4 \pm 0.27$ | $3.8 \pm 0.16$ |
| | 38 | $36 \pm 1.3$ | $31 \pm 1.1$ |
| $Ce(NO_3)_3$ | 2.0 | $1.80 \pm 0.013$ | $1.66 \pm 0.096$ |
| | 14 | $12.6 \pm 0.43$ | $12.9 \pm 0.63$ |
| | 26 | $23.0 \pm 0.96$ | $25.92 \pm 0.065$ |

The degree of sedimentation in the $CeO_2$ NP stock suspensions was assessed by measuring the cerium concentration at time intervals using ICP-MS, see figure 15. The cerium concentration at t=$-24$ h was expected to be 81 mg/L, based on the concentration of $CeO_2$ NPs and the atomic mass of cerium and oxygen. Due to visual observation of sedimentation in the tubes, a clear reduction in concentration was expected with time. This was the case for most samples. For sample A, there was an increase in measured concentration from t=0 h to t=72 h, and for sample E there was an increase from t=$-24$ h to t=0 h. The results are discussed in section 5.1.

## 4.2 Liquid media effect on nematode growth

The effect of the liquid media on nematode health was assessed by a simplified toxicity test setup. An age synchronized culture of GRX nematodes was cultured in three different liquid media; MHRW, MHRW with cholesterol, and S-base with cholesterol. The nematode length was measured after 72 h, and the results are shown in figure 16. The differences in growth were all statistically different (p<0.0001).

## 4.3 Standard toxicity test

The dose-response for $CeO_2$ NPs and $Ce(NO_3)_3$ exposure was assessed in a 96 h chronic toxicity test. The endpoints growth, fertility and reproduction were measured after exposure to a range of cerium concentrations. The results are
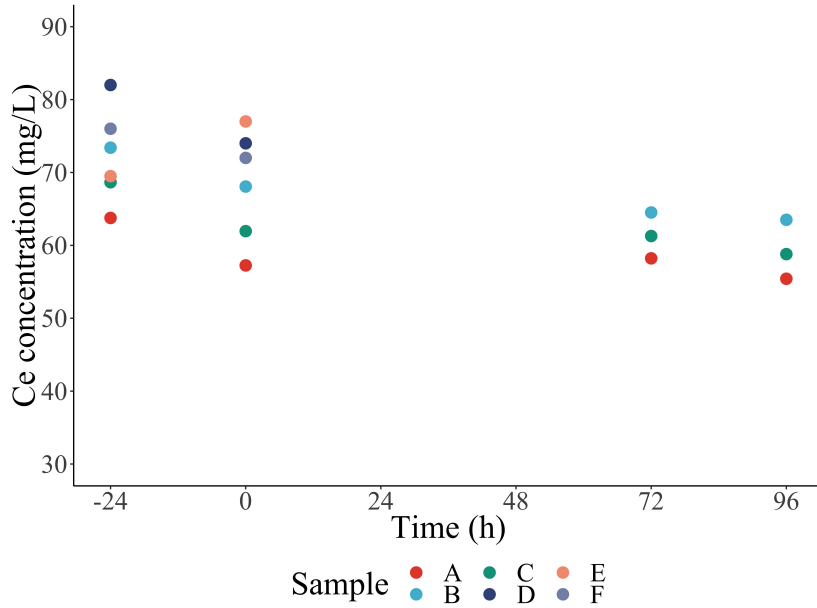
**Figure 15:** Ce concentration in CeO$_2$ NP suspensions in MHRW. Six different samples were measured using ICP-MS at different time points. Sample A, B and C are pseudo-replicates from one stock suspension, sample D, E and F from another stock suspension. The time values correspond to the toxicity test, which was started at t=0 h and ended at t=96 h for the N2 toxicity tests. Note that the y-axis start at 30 mg/L for increased readability.
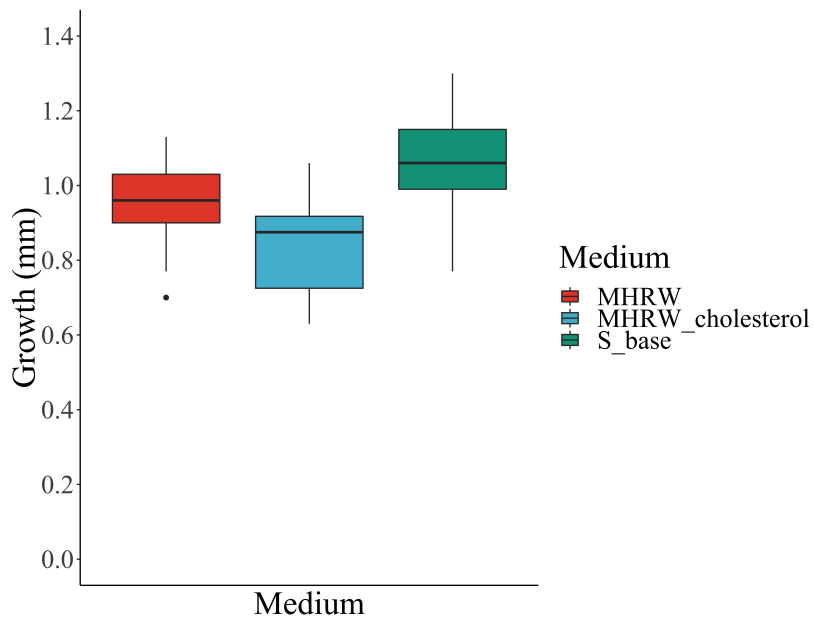


**Figure 16:** Length of synchronized GRX nematodes at t=72 h for cultures grown in three different liquid media; MHRW, MHRW with cholesterol, and S-base with cholesterol. N=20 − 40, p<0.0001 between all groups.

presented in figure 17. For the ion exposure, reproduction was the most sensitive endpoint, followed by growth and lastly fertility.

For the $Ce^{3+}$ exposure, a significant reduction in growth was seen compared to control for all exposure groups except the lowest concentration of $2\,mg/L$ cerium. Significant decrease in fertility was observed for all exposure groups from $14\,mg/L$. At the lowest exposure concentration of $2\,mg/L$, a significant increase in reproduction was seen, with a significant decrease for all other exposure groups.

For the $CeO_2$ NP exposure, there were no significant differences between the growth for control and exposure groups. However, statistical analysis showed significant differences between exposure groups; the nematodes were shorter after exposure to $4.1\,mg/L$ cerium than exposure to 1.0, 8.1 or 33 mg/L cerium. Nematodes exposed to $16\,mg/L$ cerium were also shorter than nematodes exposed to $1.0\,mg/L$ cerium. No effect was seen on fertility; all exposure groups had 100 % fertility.

For NP exposure effects on reproduction, there was a significant reduction at $4.1\,mg/L$ and $8.3\,mg/L$. There was a reduction at the subsequent exposure group of $16\,mg/L$, but the effect was not significant (p=0.054). At higher concentrations ($33\,mg/L$ cerium), no effect was seen. These results are discussed in further detail in section 5.2.

## 4.4   Oxidative stress response

To assess a possible change in ROS production and oxidative stress, toxicity tests were performed with the reporter strain SOD-1 and the biosensor strain GRX. The results from the SOD-1 assay are shown in figure 18. As described in section 3.6 and further discussed in section 5.3, these results do not qualify for statistical analysis due to nematode culture issues. The results are included as a proof of principle, and should be performed again to obtain results for statistical analysis. Figure 19 show examples of analyzed images of nematodes from each exposure group. The reduction in nematode length with increasing cerium concentration from $Ce(NO_3)_3$ can be seen, especially at $11\,mg/L$ cerium.

The results from the GRX assay are shown in figure 20. For the $CeO_2$ NP exposure, no effect can be seen at t=72 h. Unfortunately, the $33\,mg/L$ cerium exposure group is not included at t=72 h due to microscope software problems, and there is a possibility for an undiscovered effect at high concentrations. At t=48 h, there is a small but significant increase in the oxidized over reduced ratio for the $8.3\,mg/L$ and $33\,mg/L$ cerium exposure groups. For the $2.1\,mg/L$ cerium exposure group, the increase was not significant (p=0.17). For the $Ce^{3+}$ exposure, no significant differences between control and exposure groups were seen. These results are discussed in detail in section 5.2. Images of nematodes from each exposure group are shown in figure 21, and the small differences in oxidized over reduced levels of glutathione are not possible to observe qualitatively by visual inspection. A reduction in length with increasing cerium concentration from $Ce(NO_3)_3$ can be seen, especially at $10\,mg/L$ cerium.
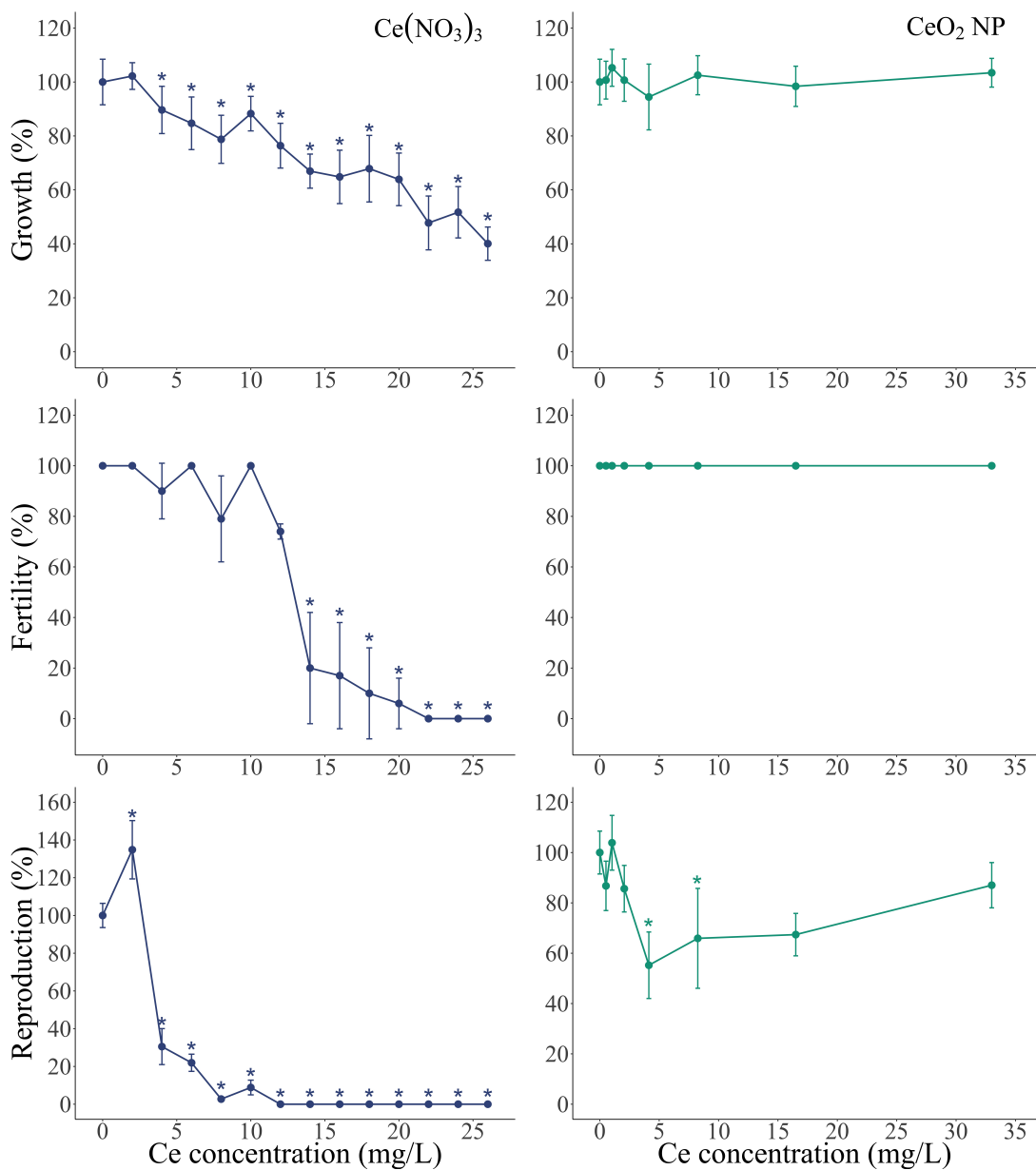
**Figure 17:** Growth, fertility and reproduction of *C. elegans* after exposure to $Ce(NO_3)_3$ (left) or $CeO_2$ NPs (right). Mean $\pm$ 1 standard deviation, all values normalized to the control. Asterisk ($*$) indicate a significant difference ($p < 0.05$) between the exposure group and control (Tukey's HSD).
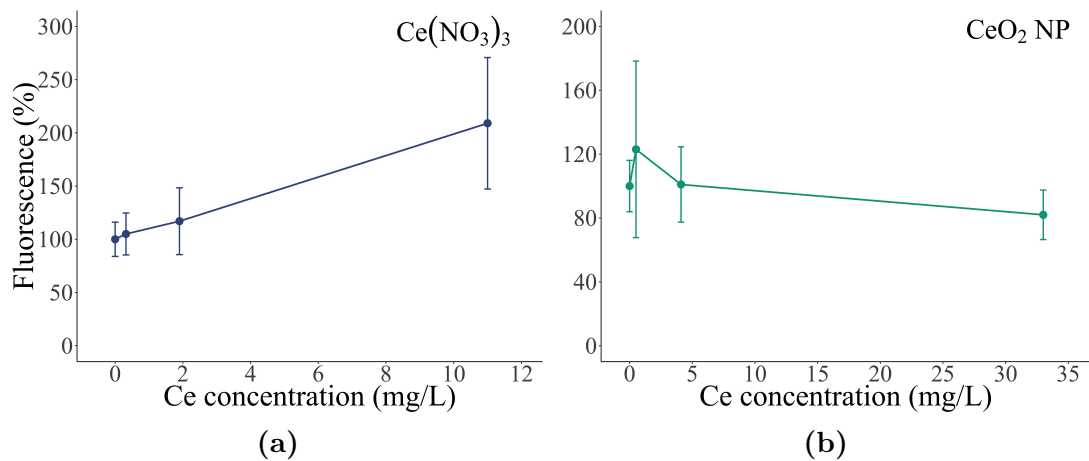
**Figure 18:** Fluorescence signal from SOD-1 nematodes after exposure to $Ce(NO_3)_3$ (left) or $CeO_2$ NPs (right). All values have been normalized by nematode size. N=5−9. No statistical analysis was performed on these data due to nematode culture issues and small sample size.
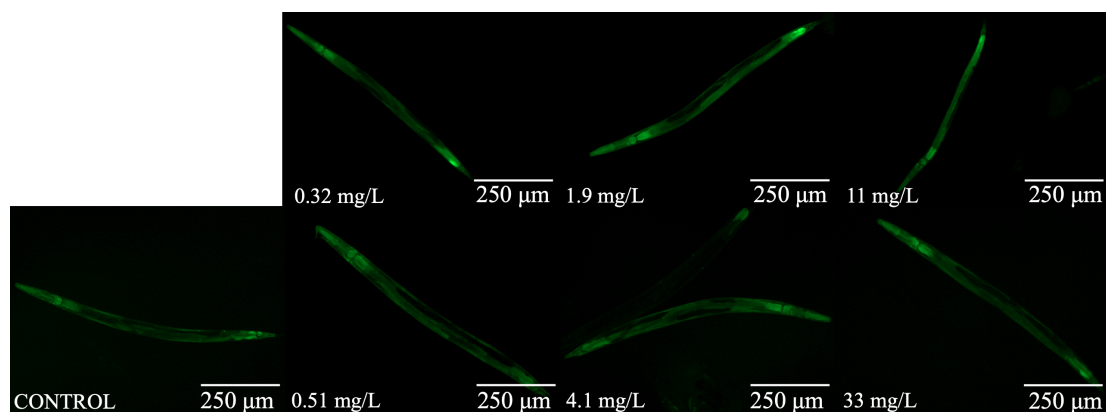


**Figure 19:** Images of SOD-1 nematodes from each exposure group of $Ce(NO_3)_3$ (top) or $CeO_2$ NPs (bottom). Control group at the bottom left.
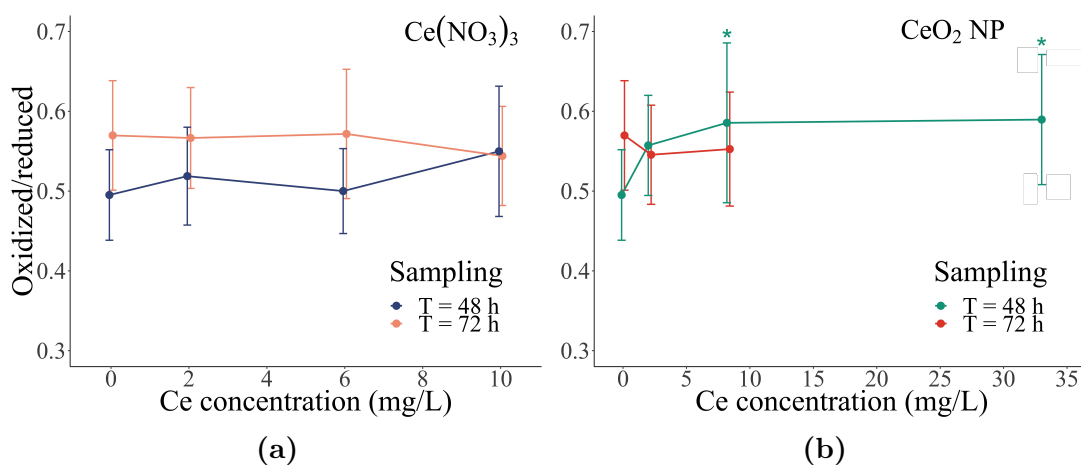
**Figure 20:** Oxidized over reduced fluorescence signal from GRX nematodes after exposure to $Ce(NO_3)_3$ (left) or $CeO_2$ NPs (right). The $33\,mg/L$ cerium $CeO_2$ NPs exposure group is not included due to microscope software problems. Asterisk ($*$) indicate a significant difference ($p < 0.05$) between the exposure group and control (Tukey's HSD). Note that the y-axes start at 0.3 for increased readability.
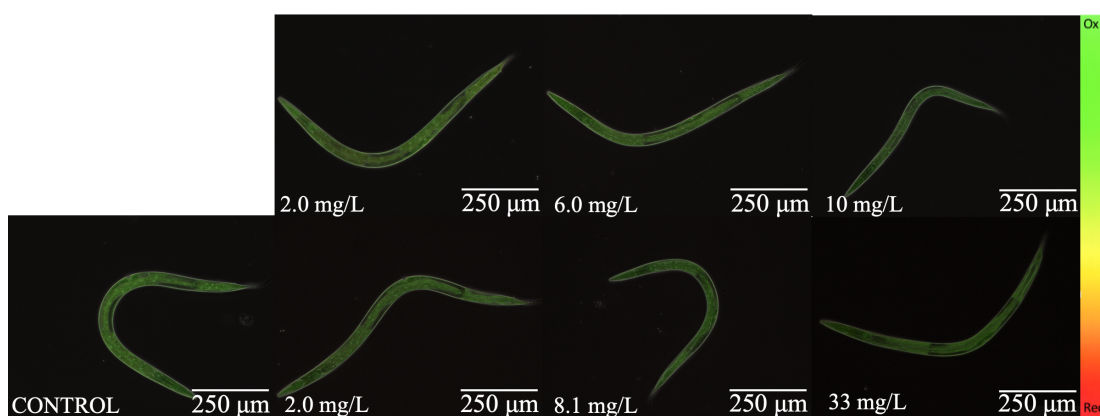


**Figure 21:** Images of GRX nematodes from each exposure group of $Ce(NO_3)_3$ (top) or $CeO_2$ NPs (bottom) imaged at t=48 h. Control group at the bottom left. Color scale from oxidized (green) to reduced (red) form of glutathione to the right. The images are constructed by overlaying the phase contrast and fluorescence channels.

# 5 Discussion

## 5.1 Exposure conditions

**Nanoparticle characteristics**

As stressed throughout this thesis, characterization of the NPs and exposure conditions is of utter importance when performing a classical toxicological assessment of NP suspensions. In this work, the NPs were characterized with respect to size distribution and zeta potential. The size distribution is important for the toxic potential, and NP toxicity have been shown to depend greatly on NP size [4]. The zeta potential indicates the stability of the NPs in suspension, which influence the degree of agglomeration and consequently the exposure of single NPs to the test organisms. Agglomerates may exhibit a different toxic mechanism, or may sediment and decrease the exposure dose.

Figure 14 shows the size distribution for NPs as measured by TEM and NTA. The size was specified to be $<25$ nm by the manufacturer, but no information on the measurement technique was given. In this thesis, the maximum Feret diameter was used for the TEM micrograph analysis, giving a distribution skewed to the right compared to a distribution based on *i.e.* the minimum Feret diameter or a mean value. Considering this, the measured values are in good accordance with the specified size. The TEM results illustrate the primary particle size and the large variance in size between individual NPs. This is also illustrated in figure 13, where the wide distribution of both NP size and shape is evident. This seem to be the case for common commercial $CeO_2$ NPs, as the EU reference material imaged during the project thesis showed similar properties. The variation in NP size and shape makes the interpretation of the toxicity assessment more challenging. In addition to the known dependency of size, the shape can affect the surface properties and the toxic potential [88].

The NTA results are valuable due to the insight into the NP behavior in aqueous suspension, and the obtained NP size is expected to be larger than for that obtained from TEM. The large increase in values support the hypothesis of substantial agglomeration of the NPs in aqueous suspension. The NTA was performed on samples of NPs in MHRW, diluted in $ddH_2O$ immediately prior to measurements. In the TEM micrographs in appendix B, agglomeration is clearly seen in the samples of NPs in both $ddH_2O$ and MHRW T. It should be stressed here that the samples measured by NTA were not treated identically to the samples used for the toxicity tests. They were not continuously stirred due to the transportation to NanoLab in Trondheim, and this might have affected the agglomeration process.

The zeta potential measurements in table 3 indicate that the NPs have a negatively charge in MHRW and MHRW T, and the suspensions are fairly unstable. In addition to the size characterization and visual observation of sedimentation in stock suspensions, this supports the evidence of substantial agglomeration. The suspension in $ddH_2O$ was found to be stable, however $ddH_2O$ is not suited as

an exposure media for toxicity testing due to the biochemical requirements for healthy nematodes. Patil *et al.* investigated the protein adsorption and cellular uptake of $CeO_2$ NPs a function of zeta potential. They found negatively charged NPs to adsorb few to no proteins, while these particles showed the highest degree of cellular uptake [89]. The zeta potential of metal oxides are affected by pH, conductivity and concentration of media components, and varying these parameters will affect the NP stability [90]. This will again affect the agglomeration rate and exposure dose, in addition to the rate of cellular uptake. The cellular uptake of the NPs was not investigated in the current work. It was hypothesized to be very low, due to the lack of observed toxic effect during the project work. However, the toxic results identified in this work imply that the degree of cellular uptake should be investigated in further research.

**Exposure media**

For NP suspensions, the liquid medium greatly affects the toxic potential of the NPs. As mentioned in section 2.4, the choice of liquid medium has been shown to cause a 100-fold difference in the measured toxic concentration range [52]. Results from toxicity assessments should therefore always be accompanied by a detailed description of the exposure medium. The choice of liquid medium in this work was moderately hard reconstituted water, as it has been shown to be a good choice for the toxicity assessment of NPs. Its advantage over traditional media such as NGM, M9 or K-medium is the lower IS. The lower concentration of simple ions in solution reduces the screening of the Coulomb forces and reduces the agglomeration, enhancing the stability [25]. However, in the present work MHRW is shown to cause substantial agglomeration of $CeO_2$ NPs, and one should investigate the possibilities for improving the choice of liquid media even further. As living organisms, *C. elegans* have certain requirements for the pH conditions and ion concentrations. The medium should be chosen as a compromise of the requirements for optimal NP stability and nematode health.

Figure 16 shows the effect of different liquid media on nematode growth. S-base with cholesterol is the medium producing the largest nematodes, and is an excellent choice of culture medium between toxicity tests. During toxicity tests, the relatively high content of salts, especially chloride, make it a suboptimal choice. Among the two other tested media, MHRW and MHRW with cholesterol, MHRW produced the longest nematodes. This was unexpected, as cholesterol ensures normal nematode development, and is required for multi-generational experiments. The reasons behind the unexpected results are not known. The small p-value (p<0.0001) demonstrate a true difference in growth between the two media. The effect of cholesterol on NP stability was not known, and therefore cholesterol was not added to the toxicity media in this work. The results in figure 16 indicate that this had no severe effect on nematode health and supports this decision.

After preparing MHRW for the toxicity tests, the measured pH should be between 7.4 and 7.8. If the pH is too high, $HNO_3$ can be added until the pH

is within the right range. By using $HNO_3$, the content of relevant ions is not increased, and its addition should have no effect on the toxicity test. With time, however, the pH in the MHRW changes due to the dynamic process of $CO_2$ absorption from and release to the surroundings. The pH is known to potentially affect the toxic potential of chemical compounds [91]. The pH of the MHRW stock solution was not measured immediately before use in the toxicity test, nor in the wells during the toxicity test. The pH could affect the results and the reproducibility of the toxicity test. To avoid this, one could make fresh MHRW before every new toxicity test, adjusting the pH to the same value each time. The pH could also be measured in dedicated wells during the course of the test, to observe potential changes *ie.* due to the addition of *E. coli* and *C. elegans*.

**Cerium concentration**

To assess the real concentrations of cerium during the toxicity test, ICP-MS measurements were preformed for the N2 assays E2 and E3. Triplicate samples from the lowest, the highest and a medium concentration group were measured at t=0 h and t=96 h. The results for E3 are listed in table 4. For the ion exposure groups, the real cerium concentrations in the samples are very close to the calculated values, with minimal differences caused by pipetting uncertainty, adsorption of cerium to the plastic wells, or evaporation of liquid. This was confirmed by the ICP-MS results at both t=0 h and t=96 h for all ICP-MS measurements (E1, E2 and E3). For the ion exposures, the purpose of the ICP-MS measurements was mainly as a control of the preparation of dilution solutions, more than an investigation of the cerium behavior in the exposure media.

For the NP suspensions however, the ICP-MS measurements were a central part of the exposure characterization. Table 5 in appendix C show the ICP-MS results from E2, and is included to demonstrate the varying results between E1, E2 and E3. In E1 and E3, the cerium concentrations in the NP samples were very similar at t=0 h and t=96 h. The results indicate that the sampled aliquots at t=0 h have a cerium concentration around 80 % of the initial cerium concentration in stock suspensions. For E2 however, there was at least a 50 % reduction in all three NP exposure groups from t=0 h to t=96 h. A possible explanation is that a large fraction of the NPs adhered to the plastic wells, due to some circumstances that were not present during E1 or E3. Another possibility is that the mixing of the content in the wells with the pipette before sampling was not done thoroughly. However, one would expect that to produce similar effects for the ion samples, which was not the case. The SD of the NP samples were small at both time points, so the results seem to be representative of the true concentrations.

The analysis of the endpoints growth, fertility and reproduction for the $Ce^{3+}$ exposed nematodes in E2 revealed a dose-response that deviated markedly from E1. The analysis was therefore terminated. The drastic lowering in cerium concentration for $CeO_2$ NP samples from t=0 h to t=96 h, combined with the deviating does-response for $Ce^{3+}$ samples, indicate an issue with the exposure media.

Possible issues include a deviating pH, contaminations, or deviating content of *eg.* Tween 20 or *E. coli.* Based on the available knowledge, it is not possible to conclude on the reason for the deviating ICP-MS results. However, it worked as a strong reminder of the importance of exposure characterization, and the strongly advised need for replicate experiments to expose experimental deviation.

Figure 15 presents the cerium concentration in six samples from two $CeO_2$ NP stock suspensions, at four time points after preparation. The estimated concentration immediately after preparation (t=−24 h) was $81\,mg/L$, based on the added amount of $CeO_2$ NPs and the atomic weight of cerium. Figure 15 shows a high variation in the concentration at t=−24 h, ranging from around 65 to 85 mg/L of cerium. The internal variation between the three pseudo-replicates from one stock suspension is smaller than the variation between all six samples. As a reference point, the ICP-MS results of the cerium concentrations in E3 (table 4) have small SDs, indicating small measuring and instrumental errors. The variations in figure 15 are therefore assumed to be caused by true differences in the stock suspensions. With time, most samples experienced a reduction in concentration. This was expected as a consequence of agglomeration and sedimentation, as indicated by several observations.

The increase in concentration in two of the samples between two time points was unexpected. As mentioned in section 3.1, NP samples were always pipetted from the $5\,mL$ mark in the stock tubes. Due to the visual observation of sedimentation, the concentration of cerium was presumed to be lowest at the surface, with a gradual increase towards the bottom. By always sampling from the same mark, the variations in cerium concentrations should be minimized. However, it is reasonable to assume that the agglomeration and sedimentation process differ slightly between samples due to small differences in *e.g.* concentration of NPs, Tween 20 or contamination. In addition, the sampling of NPs and NP agglomerates will always be subject to random differences in the pipetted samples. If the suspension is highly agglomerated, the difference of a few agglomerates in the pipetted samples can produce a notable difference in the measured concentrations. The large variation between the samples are therefore believed to reflect the real concentrations in the sampled aliquots for ICP-MS measurements. The increase in two samples between two time points is believed to be due to the same reasons, and are also thought to reflect the real concentrations in the sampled aliquots.

## 5.2   Dose-response and mechanisms of toxicity

**Standard toxicity assessment**

Chronic toxicity tests were performed on three strains of *C. elegans*; the wild type N2, the reporter strain SOD-1, and the biosensor strain GRX. The results from the N2 toxicity test are shown in figure 17. The control values for growth, fertility and reproduction were well within the expected range, indicating a robust experiment (results not presented). The dose-response curves for $Ce^{3+}$ exposure

were as expected, with reproduction as the most sensitive endpoint, followed by growth and lastly fertility. For reproduction, an increase was observed at $2\,\mathrm{mg/L}$ cerium, and a reduction for all other concentrations. Low-dose stimulation with high-dose inhibition is an effect known as hormesis. Hormesis is a well known and common effect for environmental stressors such as toxic compounds, and is described as an adaptive response to a moderate stress [92, 93].

Fertility demonstrated the largest variance of the three endpoints, after $Ce^{3+}$ exposure. Fertility is measured for each nematode as a Boolean (logical) value; either the nematode is gravid or it is not. With around 10 nematodes in each well, the difference of one or two gravid individuals between replicates will greatly affect the variance of fertility. This is in contrast to growth, which is measured by continuous length, or reproduction, measured by a large number of offspring per nematode (around 60 for the control). The inherent variance in susceptibility in a population may cause a larger variance in fertility, compared to growth or reproduction. Despite the relatively high variance for fertility, the low variance in growth and reproduction indicate a robust experiment.

During the project work, a toxicity test was performed for the endpoints fertility and reproduction for an overlapping range of $Ce^{3+}$ concentrations (0 to 700 mg/L cerium). The dose-response curves for E1 and E3 are plotted together in figure 24 in appendix D, showing very similar dose-response curves for the two experiments. The similarity a high reproducibility of the toxicity test. The deviating results in E2 indicate the opposite, but this is believed to originate in an issue with the exposure medium, as discussed in section 5.1. In E1, 100 % mortality occurred between the two tested concentration of 22 and 44 mg/L cerium. In E3, growth was reduced to 40 % for $26\,\mathrm{mg/L}$ cerium, while both fertility and reproduction were reduced to 0 %. Hence, the biological malfunction at $26\,\mathrm{mg/L}$ cerium seem to be approaching the limit for mortality of the nematodes.

For the $CeO_2$ NP exposure, no effect was observed for fertility for any concentration. For reproduction, a significant decrease was seen for the two intermediate concentrations of 4.1 and 8.1 mg/L cerium. A non-significant reduction was seen at the following exposure concentration of $16\,\mathrm{mg/L}$ cerium, while there was no observed effect at the highest tested concentration of $33\,\mathrm{mg/L}$ cerium. During E1, no effect was seen on reproduction for the same concentration range. Previously, researchers at CERAD have demonstrated a small reduction in growth and fertility for 5.5 and 17 mg/L cerium, with no effect at higher concentrations and only weak evidence of decreased reproduction [94]. The difference in results from the same laboratory indicates difficulties with the reproducibility of the experimental setup. The lack of observed effect during E1 may also be attributed to the authors current lack of experience with the laboratory techniques, which may have caused larger variations and more errors.

The results for growth after $CeO_2$ NP exposure revealed some interesting trends. No significant differences were observed between the control and exposure groups. However, there were significant differences between several exposure groups; the nematodes were shorter after exposure to 4.1 mg/L cerium than ex-

posure to 1.0, 8.1 or $33\,\mathrm{mg/L}$ cerium. Nematodes exposed to $16\,\mathrm{mg/L}$ cerium were also shorter than nematodes exposed to $1.0\,\mathrm{mg/L}$ cerium. The growth for the lowest tested exposure of $1.0\,\mathrm{mg/L}$ cerium had a slightly higher mean and slightly lower variance than the control group, which led to the lower p-values for the difference between other exposure groups. Re-doing the experiment with a larger sample size might reveal significant differences also between the control and exposure groups. With this in mind, the results provide indications of a reduction in growth for $4.1\,\mathrm{mg/L}$ cerium, in good accordance with the reduction in reproduction. The weak evidence for reduced growth is in line with growth being a less sensitive endpoint than reproduction. The lack of effect on growth for $33\,\mathrm{mg/L}$ cerium is also in good accordance with the reproduction results. The combined results for reproduction and growth indicate that the range of toxic concentrations for $CeO_2$ NPs under these exposure conditions is around $4.1\,\mathrm{mg/L}$ to $16\,\mathrm{mg/L}$ cerium. The lack of effect at higher concentrations support the hypothesis of substantial agglomeration, as discussed in section 5.1.

**Toxic mechanisms of action**

The challenges experienced for the SOD-1 toxicity assays (E4 and E5) are discussed in detail in section 5.3. The results presented in figures 18 and 19 are included as a proof of principle, and are not discussed further.

The GRX assay revealed interesting differences between $Ce^{3+}$ and $CeO_2$ NP exposure. Following $Ce^{3+}$ exposure, no effect on the oxidized over reduced form of glutathione was observed for any of the concentrations. Oxidative stress response after exposure to $Ce^{3+}$ has been previously reported by Kawagoe *et al.* in mouse liver. They reported an increase in metallothionein synthesis and glutathione levels after chronic exposure to $Ce^{3+}$, indicating an oxidative stress response [95].

Oxidative stress and the cellular processes to keep a healthy redox balance are very complex, and one should be careful when drawing conclusions regarding ROS production and oxidative stress response from the results of only one transgenic strain. The ratio of oxidized over reduced glutathione has been described as a proxy for the total cellular redox state [96]. Recent investigations indicate that this might need some moderation, and that one should be more cautious when interpreting a change in the ratio [97]. However, the obtained results does not give any indications of a disruption in the cellular oxidative stress caused by $Ce^{3+}$ exposure. Re-doing the SOD-1 assay with a new nematode culture would lead to added insight into the mechanisms of $Ce^{3+}$ toxicity.

Other possible MOAs for $Ce^{3+}$ toxicity are not investigated in this work, but possible MOAs reported by others include enzyme inhibition, disruption protein synthesis or agglomeration of membrane proteins [43, 46, 47]. Another possible MOA is the competition of cerium with essential metals. Ma *et al.* reported chronic toxicity after $Ce^{3+}$ exposure to *Daphnia magna* [48]. They suggested this to be due to the possible competition between $Ce^{3+}$ and $Ca^{2+}$, although this was not confirmed. $Ce^{3+}$ and $Ca^{2+}$ are similar in size, and although they have different charges, $Ce^{3+}$ can possibly bind to $Ca^{2+}$ cellular binding sites [98].

Likewise, $Ce^{3+}$ can possibly compete with $Fe^{3+}$, which are different in size but have the same charge. *C. elegans* do not produce hemoglobin, but the dietary heme is incorporated into other hemeproteins, since free heme is hydrophobic and cytotoxic. $Ce^{3+}$ can possibly compete with $Fe^{3+}$ in these hemeproteins, interfering with oxygen transportation [99]. Competition with essential metals is a common MOA for metal toxicity [4].

For the $CeO_2$ NP exposure, a small but significant increase was observed for the two highest tested concentration. The dissimilarity in the toxic concentrations for N2 and GRX are not known, but might be due to differences in the agglomeration processes in E3 and E7. The results might also indicate a particle-specific toxicity for NP agglomerates at high concentrations that was only observed for GRX. Different strains also have different sensitivities, and this could be investigated further by testing more concentrations in the tested range for both N2 and GRX. The evident difference between $Ce^{3+}$ and $CeO_2$ NP exposure indicate a nano-specific MOA.

This hypothesis is further supported by the indications of highly inert NPs. During the project work, the NP samples were acid digested to decompose the ions using two different treatments. In the mildest treatment, the samples were mixed with Ultrapure $HNO_3$ and left at 60 °C overnight and then at 90 °C for 1 hour. The more effective treatment was the same used in this thesis, using a microwave digestion system and exposing the samples to 260 °C and 40 bar. For the samples digested using the mildest treatment, ICP-MS results showed around 10 % of the cerium concentration found in the samples treated using the effective treatment. Withstanding a treatment with acid at 60 and 90 °C so effectively, indicates very table and inert NPs. Hence, very few ions are supposed to be released during the toxicity test at 20 °C, in good accordance with literature [24]. The ion concentration in the NP exposure samples are thus assumed to be low, and the observed toxic response indicates a nano-specific MOA.

The redox potential of $CeO_2$ NP is believed to originate in the considerable fraction of oxygen vacancies, allowing for cycling of cerium surface atoms between the $Ce^{3+}$ and $Ce^{4+}$ oxidation state. This redox potential enables $CeO_2$ NPs to function as an electron donor or acceptor, depending on the specific conditions. The properties and mechanisms behind this should be further investigated in future work.

The results for $CeO_2$ NP exposure to GRX are also valuable as a reminder of the need of repeated analysis. This is not only true for the characterization of dynamic NP behavior, but also for the complex dynamic process of cellular oxidative stress. The analysis at t=72 h showed no differences in the ratio of oxidized over reduced glutathione, and the effect would not have been discovered if analysis had not been performed at t=48 h.

Other contributing MOAs in addition to ROS production cannot be ruled out. Possible contributions include nematode cuticle loss as reported by Lahive *et al.* for the earthworm *Eisenia fetida* [56]. Arnold *et al.* suggested that part of the effect could be attributed to the agglomeration of $CeO_2$ NPs with the *E. coli*

food source [59]. The non-spherical shape of the NPs investigated in this work might also be hypothesized to cause mechanical damage to either the nematode cuticle or cellular membranes inside the gut. In this work, the degree of uptake and bioaccumulation of $CeO_2$ NPs was not investigated.

Others have reported a lack of observed effect on oxidative stress response. Roh *et al.* investigated the toxic effect of $CeO_2$ NPs of different sizes on N2 nematodes, by measuring the expression of genes coding for proteins that are important in a stress-response, including *sod-1* and *ctl-2*. They did not observe any significant differences for the redox-related genes, and the xenobiotic metabolism enzyme coded by *cyp35a2* was the only one showing a profound increase in expression [100]. Another possible indirect MOA is the adsorption of nutrients such as phosphate to the NPs, decreasing the available concentration for *C. elegans* uptake [101, 102].

In an ecosystem exposed to $CeO_2$ NPs, the $CeO_2$ NPs might affect the toxicity of other environmental pollutants, either due to synergistic effects or by the adsorption of *ie.* PAHs to the NPs, as reported for CNTs and $TiO_2$ NPs [17–20]. This possibility was not investigated during this work. Until a deeper understanding of $CeO_2$ NP toxicity is achieved, the complexity of experimental setups should be minimized. In the future, the potential effects of $CeO_2$ NPs in combination with other toxic compounds could provide important insight into ecologically relevant exposure conditions.

## 5.3    Experimental challenges and critique

### SOD-1 culture issues

As mentioned in section 3.6, there were issues with the SOD-1 culture during both E4 and E5. During E4, the main issue was too few nematodes per exposure group. For N2 toxicity tests, around 10 nematodes were exposed per concentration. Due to the differences in analysis procedures, each exposure group should contain around 50 nematodes for SOD-1 and GRX experiments. The increase in the number of individuals is not assumed to affect the results, as the available food, space and oxygen is assumed to be enough for 50 nematodes without introducing substantial competition among individuals. In E5, the number of nematodes was suitable for analysis. However, the imaging revealed large individual differences in fluorescence protein expression, as illustrated in figure 22. Both panels (a and b) in figure 22 are from the control group imaged at t=72 h. In (a), a normal distribution of fluorescence protein expression is observed, showing a high degree of expression in the head and tail, with some expression in the rest of the body. In (b), only a small part of the tail was bright fluorescent. This issue was either not present during E4, or was not recognized due to the small number of nematodes per sample.

Attempts were done to fix the problems to allow for a new toxicity test with robust results, but were not successful. The problems appeared to be so persistent that it could only be solved by requesting a new nematode culture. Due to the
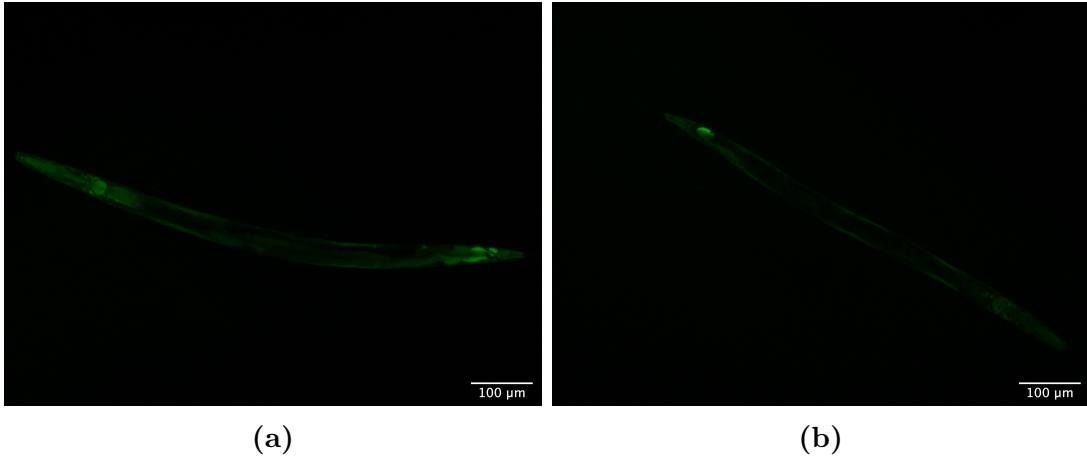
<div align="center">(a)        (b)</div>

**Figure 22:** Fluorescence microscopy images of SOD-1 nematodes at t=72 h.

delivery and transportation time, it was not possible to perform a new toxicity test during this work. The following paragraphs describe the unsuccessful attempts to fix the culture issues.

As mentioned in section 2.5, SOD-1 nematodes move in a different way from wild type *C. elegans*. The rolling movement of SOD-1 nematodes is less efficient than the non-rolling movement of wild type *C. elegans*, and they spend more energy on finding food. Occasionally, homologous recombination lead to the loss of the gene coding for the rolling movement and GFP signaling, and these individuals outperform the rollers. After a few generations, the culture is full of nematodes that do not contain the GFP gene, and this culture is no longer suited for use in toxicity tests. Fortunately, this effect can easily be spotted when observing the movement of the individuals in the culture, which allows for careful separation of rollers and non-rollers.

This was done by the following procedure: NGM plates were seeded with *E. coli* by preparing a liquid culture of *E. coli* as described in section 3.6. After incubation, 2 mL of the liquid *E. coli* culture was pipetted onto NGM plates. A few mL liquid culture of SOD-1 was pipetted onto a prepared NGM plate and left to incubate until a sufficient number of adult nematodes were present. Under the stereo microscope, a sterilized inoculation loop was used to transfer rollers one by one onto a fresh NGM plate. The new plate was observed under the microscope daily. L1 stage larvae tend to cling to the adult nematodes, and may be transferred along. Even a few non-rollers will multiply and destroy the culture. The movement patterns in the NGM reveal if any living non-rollers are present, and these can be killed using a glowing inoculation loop. This procedure should result in a culture of only rollers, that can be cultivated until enough nematodes are present to perform a toxicity test.

However, this did not solve the culture problems in this case. Fluorescence microscopy of the new culture revealed that the fluorescence signal from the nematodes was still very varying between individuals. Without a consistent control

group or background level of fluorescence, a new toxicity test would not have provided useful results. Others have experienced similar issues with the reporter strain SOD-3, which were only solved upon re-ordering the strain (personal communication with Lisa Rossbach). Due to the unsuccessful attempts to fix the culture, analysis was performed on the results from E5. Images of nematodes resembling the individual in (a) were manually picked for analysis, while images deviating from this, such as the one in (b), were ignored. This resulted in a low number of nematodes per exposure group (N=5-9). The results are presented in figures 18 and 19 as a proof of principle, but no statistical analysis was performed. In future work, the experiment should be performed using a new culture to obtain useful results.

**Fluorescence imaging bias**

For the GRX imaging, controls were measured both before and after imaging of the cerium exposure groups, imaging 23 and 19 nematodes from control samples, respectively. The oxidized over reduced ratios between the two control groups were significantly different (p<0.001). The post-imaging control group was chosen as the control group for comparison with the exposure groups. This was done based on three factors; the higher number of nematodes imaged in this group, the lower standard deviation, and the higher oxidized over reduced ratio. For the exposure groups, SDs ranged from 0.05 to 0.08. For the pre-imaging control group, the SD was 0.13, while for the post-imaging control group it was 0.06. More outliers are supposed to have been measured in the pre-imaging control group, and the post-imaging control group was assumed to better reflect the values of the imaged nematodes. Potential stress on the nematode samples waiting for imaging, *e.g.* caused by reduced oxygen levels in the wells, could possibly disturb the internal redox balance as discussed by Braeckman *et al.* [35]. To avoid this, the control value from the end of imaging should be used. This should minimize the risk of incorrectly interpreting an increase in oxidized over reduced ratio for exposure groups as a true difference, when this might not be the case.

As mentioned in section 3.6, nematodes tended to burst during imaging due to the pressure from the cover slip. At t=48 h, the frequency of bursting could be minimized by effective imaging. After placing the cover slip on the microscope slide, most nematodes did not burst within the first 2-3 minutes. At t=72 h however, the bursting began almost immediately after placing the cover slip. Nematodes that have burst are not suited for image analysis and fluorescence quantification, and imaging was continued until a sufficient number of nematodes were imaged (N=24 at t=48 h and N=18 at t=72 h). Based on the authors experience, bursting affected larger nematodes at a higher rate than smaller nematodes. This led to an unwanted bias, as smaller nematodes were possible to image at a higher frequency than larger nematodes. It is possible to assume that a higher fraction of the smallest nematodes were extra susceptible individuals, when compared to the population average. In that case, the biased imaging would lead to a biased quantification of fluorescence, overestimating the toxic effect. Several

measures were taken to try to minimize the bursting, none of which were very successful. The attempts are briefly described in the following paragraphs.

One attempt was to make agar pads by melting agarose in $dH_2O$ by the method described by Duncan Ledwich *et al.* [103]. Placing the nematodes on the agar pad before placing the cover slip would reduce the pressure on the nematodes, but the process of making the agar pads was difficult to do satisfactory. The agar pads were very loosely attached to the microscope slide, and tend to slide off. The preparation of a substantial amount of microscope slides, before wrapping and storing them separately to avoid evaporation and drying of the pads, was considered to be too difficult and time-consuming to pursue.

Another attempt was to make use of two cover slips as spacers between the microscope slide and cover slip. This led to issues such as liquid being drawn under the side cover slips, causing more and not less pressure to the nematodes. This was attempted to be solved by adding drops of MHRW T to the microscope slide before placing the spacer cover slips. This improved the setup, but the arrangement did not contribute noticeably to a reduction in bursting. Following these unfruitful attempts, imaging was done by the standard method of placing the cover slip directly upon the sample. Hopefully, the biased imaging did not significantly affect the results. In future experiments, more attempts could be done to optimize the imaging procedure to avoid this problem.

## Applicability of standard toxicity tests on NPs

The discussion of exposure conditions in section 5.1 demonstrate that there are several challenges with the toxicity test setup. In her PhD thesis from 2011, Nanna Hartmann raises some important questions regarding the suitability of standard toxicity tests developed for soluble toxicants, when used for the assessment of insoluble NPs [104]. Since then, these questions have been investigated further but are still highly relevant. It lies beyond the scope of this thesis to discuss this complex but important issue in detail, but a few highly relevant aspects are discussed in the following section.

Hartmann points out several issues that complicate the assessment of NPs using standard toxicity tests; non-linear relations between concentration and agglomeration, adhesion of NPs to organism surfaces and cell membranes, difficulties relating primary NP properties to observed effects, dynamic two-way interactions between NPs and organisms, and challenges in accurately describing the exposure conditions in a dynamic system. To limit the effects of these challenges, a combination of different approaches and techniques is often advised, and the essential need for thorough characterization is stressed.

The difficulties linked with using standard toxicity tests on NPs arise from the fundamental differences between soluble compounds and NPs. NPs are solid-state compounds, influenced in suspension by physical forces and interface properties. Ions are water soluble, more subject to molecular transformations [105]. These fundamental differences lead to the challenges that are encountered when performing, interpreting and presenting the results from experiments such as those

performed in this work.

The dose-response curve for reproduction after $CeO_2$ NP exposure in figure 17 illustrate the challenges in using standard dose-metrics to describe the toxic dose of NPs. The presented results indicate that weight per volume is not the best suited dose-metrics for this specific experiment. Substantial agglomeration is indicated in this work, but the relation between concentration and agglomeration is unknown, and is possibly non-linear. An important aspect of NP properties is the large surface area to volume ratio, increasing rapidly with decreasing particle size. The surface area is the reactive site of any particle, and as frequently mentioned, the redox potential of cerium atoms at the surface is postulated to cause the biological effects of $CeO_2$ NP exposure. The surface area might be a more suitable dose-metric, as suggested in literature for both $SiO_2$ and $CeO_2$ [102, 106, 107]. Although the significance of surface area is emphasized in inhalation studies where increased surface area is known to cause *eg.* increased fibrogenicity, the surface area has gotten little attention within ecotoxicological research [108].

Agglomeration will cause a decrease in surface area as a consequence of the decrease in surface to volume ratio with increasing particle size. Quantifying the total surface area is challenging, and is complicated further by the vast variation in NP shapes of the NPs under investigation in this work. Estimates can be done assuming spherical particles, and using the size distribution found by TEM image analysis. Knowledge of the agglomeration process would allow estimates of the dynamic size and number of agglomerates at different time points. Integrating the exposure dose over the course of the toxicity test, the response could be presented as a function of surface area. The resulting graph may turn out to better reflect the relationship between dose and response. Another possible way of measuring dose is to estimate the degree of adhesion of the NPs, to either the organism surface or to cellular membranes upon uptake. Loss of cuticle from the body wall and reduced gut epithelium integrity for *C. elegans* as reported by Lahive *et al.* indicate that adhesion may contribute to the toxic effect of $CeO_2$ NPs [56]. To complicate matters even more, exposure volume has been shown to affect the toxic response. Increasing suspension volume, and hence the total CNT mass, caused a significant increase in uptake of CNTs in *Daphnia magna* [109].

Lastly, the dynamic nature of NP suspensions must be taken into consideration. One reason for the dynamic nature of NP suspensions is the possibility for organism effect on the NPs. Organic matter excreted from the organisms may, as other sources of NOM, affect the toxicity of metal oxides [110–112]. The dynamic character of NP suspensions mean that characterizing exposure parameters at the beginning and end of a toxicity test is not sufficient to gain a complete understanding of the conditions throughout the experiment. Repeated measurements of the exposure concentrations can be useful, but care must be taken when interpreting the results. A measured decrease in concentration during the test can indicate adsorption of NPs to the surrounding compartment, leading to a decrease in dose. It can also be caused by uptake and bioaccumulation into the organism, or adhesion to the organism surface, possibly causing toxic effect by internal or

external mechanisms, respectively. The results may therefore underestimate the exposure, and does not reveal any further information regarding the location of the NPs. This should be investigated by *eg.* a retention experiment, as described in section 5.4. Hence, concentration measurements are useful as an indication of NP stability, but not necessarily of the exposure dose.

## 5.4 Future work

As discussed throughout the thesis, the results from the SOD-1 reporter strain were affected by nematode culture issues, and should be performed again with a new nematode culture. Together with the presented results from the wild type strain N2 and the biosensor strain GRX, this would provide further insight into the suggested oxidative stress response to $CeO_2$ NP exposure. For any assay on transgenic fluorescent strains, fluorescence quantification should be performed for different nematode parts such as the head, tail and lumen of the nematode. This can reveal differences that are not detected when averaging the intensity for the full nematode. After imaging the nematodes, this is easily performed and only requires extra time for image and data analysis.

In future toxicity assays, the concentration, speciation and oxidation state of cerium in the NP exposure media should be monitored throughout the course of the experiments. Assessing the size fractions of cerium could be performed by either ultrafiltration or powerful centrifugation of the exposure media, followed by ICP-MS measurements. MHRW should be prepared with the same pH before every experiment, and the pH should be measured at different time points. The effect of cholesterol, *E. coli* and *C. elegans* on the NP suspension stability should be studied, together with the NP agglomeration dynamics. The concentration range should be chosen from the intermediate concentrations that caused toxic effects in this work, around 4 to 33 mg/L cerium. It might also be fruitful to choose only one concentration within this range, and perform extensive characterization of the exposure conditions. This could provide valuable insight into the NP properties and behavior, and could aid in improving experimental methods for further experiments. The investigations should involve experimenting with additional dose-metrics to weight per volume, such as total NP surface area.

The NP properties determining the fraction of oxygen vacancies should be characterized, and effort put into widening the understanding of the redox-potential of $CeO_2$ NPs. The oxidation state of both pristine and suspended NPs should be measured using suitable techniques.

The degree of ingestion and cellular uptake should be assessed by a retention test, with a similar experimental setup to the toxicity assays presented in this thesis. At the end of the test, nematodes should be divided into two groups and prepared for ICP-MS measurements. One group is rinsed to remove any $CeO_2$ NPs present on the nematode surface, before standard sample preparation. The other group is rinsed, and then left to eat *E. coli* in an environment free of any cerium. After two hours, the nematodes are prepared for analysis. As mentioned

in section 2.5, *C. elegans* defecate every two minutes, each time expelling around 30-50 % of the intestinal volume [66]. After two hours, any ingested NPs that were not taken up by the intestinal cells will be expelled. Knowledge of the degree of NP uptake will aid in the interpretation of toxic effects.

# 6 Conclusion

In this work, $CeO_2$ NPs were characterized and their toxicity assessed using the model organism *C. elegans*. Previous research has revealed the potential for both toxic and beneficial effects of $CeO_2$ NPs, suggested to originate from the redox-potential of the NPs. To investigate this, the oxidative stress was assessed using two transgenic strains.

The $CeO_2$ NPs were characterized with respect to size and charge. Image analysis of TEM micrographs suggested a primary particle size of around 10 nm, while NTA measurements indicated a hydrodynamic size of around 60 nm. ICP-MS measurements revealed that around 80 % of the cerium remained in the middle of the stock suspension tubes 24 hours after preparation, and the concentration continued to decrease with time. Substantial agglomeration was further indicated by the low zeta potential of around $-9.8\,mV$, and the visual observation of agglomeration in the TEM micrographs. During the toxicity test, the measured cerium concentrations in the exposure media were very similar at t=0 h and t=96 h, probably due to the mixing of the content before sampling.

Cholesterol is needed for normal nematode development, but was not added to the exposure media to minimize the suspension complexity. To investigate possible negative effects of this on nematode health, nematode growth was measured in different media with and without cholesterol. Surprisingly, MHRW without cholesterol produced longer nematodes than MHRW with cholesterol, and was confirmed to be a suitable exposure medium for *C. elegans* toxicity assays.

The wild type *C. elegans* strain experienced toxic effect from exposure to $Ce^{3+}$. A hormetic effect was observed for reproduction, the most sensitive endpoint, with an increase at the lowest tested dose of $2\,mg/L$ cerium, and a considerable decrease for all other concentrations. Growth was significantly impaired from $4\,mg/L$ cerium. Fertility was the least sensitive endpoint and was significantly decreased from $14\,mg/L$ cerium. After $CeO_2$ NP exposure, only reproduction was significantly affected compared to controls. A significant decrease was observed at 4.1 and 8.1 mg/L cerium, with a non-significant reduction for $16\,mg/L$ cerium (p=0.054). However, nematode growth war decreased for $4.1\,mg/L$ cerium compared to $1.0\,mg/L$ cerium, giving weak evidence of toxic effect also for growth. No effect was seen at the highest tested concentration of $33\,mg/L$ cerium, assumed to be caused by substantial NP agglomeration resulting in decreased NP exposure.

The transgenic trains SOD-1 and GRX were used to assess the potential redox mechanism behind the observed toxic effect. Unfortunately, no conclusions could be drawn based on the results from the reporter strain SOD-1, due to nematode culture issues. For the biosensor strain GRX, no difference in the ratio of oxidized over reduced form of glutathione was observed after $Ce^{3+}$ exposure. For $CeO_2$ NP exposure, a significant increase was seen in the ratio at t=48 h for the two highest tested concentrations of 8.1 and 33 mg/L cerium. A non-significant increase was seen for the lowest tested concentration of 2.0 mg/L cerium (p=0.17). No effect was observed at t=72 h. In addition to revealing differences in the redox

state of glutathione, imaging at t=48 h produced more robust results with a higher number of nematodes and less imaging bias than imaging at t=72 h. The difference in results between $Ce^{3+}$ and $CeO_2$ NP indicate a nano-specific MOA, caused by ROS production and oxidative stress.

As hypothesized, the results presented in this thesis support the toxic potential of $CeO_2$ NPs to *C. elegans*. The observed increase in oxidized over reduced ratios of glutathione indicate ROS production and an oxidative stress response. This seem to be a nano-specific MOA, not caused by the release of ions. The oxidative stress is believed to originate in the reported ability of $CeO_2$ NPs to act as an electron donor by the oxidation of $Ce^{3+}$ to $Ce^{4+}$, acting as a producer of ROS. A nano-specific MOA is supported by the indications of inert NPs. Other MOAs may contribute to the observed toxic effect, but this was not investigated in the present work. Lastly, the toxic response of $CeO_2$ NPs was not present at high concentrations for the N2 strain, assumed to be caused by NP agglomeration.

For NP toxicity assessment, the need for thorough characterization cannot be stressed enough. Future work should focus on characterization of NP properties and behavior in exposure media, repeatedly throughout the course of the toxicity test. This could add important insight into the toxic effects reported in this thesis. Focus should be put into the investigation of the agglomeration dynamics. The degree of NP uptake into the nematode should be assessed, in addition to the degree of NP adhesion to the organism surface. The use of standardized toxicity tests on insoluble NPs is challenging, and effort should be put into validating the experimental protocols. Thorough characterization and replicate experiments should be performed to reveal any misinterpretation of the toxic effects.

Considering the extensive use of $CeO_2$ NPs in commercial applications and the demonstrated lack of understanding of the risks and toxic effects involved, the need for continued research on this area is evident. The complexity of the field demands cooperation across different scientific fields, such as cell biology and materials science. With a comprehensive and thorough approach to this task, the ecotoxicological risks could be sufficiently investigated and documented, hopefully allowing for safe and controlled use of $CeO_2$ NPs in industry and in science.

# References

1. Sahoo, S. K., Parveen, S. & Panda, J. J. The present and future of nanotechnology in human health care. *Nanomedicine: Nanotechnology, Biology and Medicine,* 20–31 (2007).

2. Diallo, M. & Brinker, C. J. in *Nanotechnology Research Directions for Societal Needs in 2020* 221–259 (Springer Netherlands, Dordrecht, 2011). doi:`10.1007/978-94-007-1168-6_6`.

3. Scheringer, M. Environmental risks of nanomaterials. *Nature Nanotechnology* **3,** 322–323. ISSN: 1748-3387 (June 2008).

4. Walker, C. H., Sibly, R. M., Hopkin, S. P. & Peakall, D. B. *Principles of ecotoxicology* 4th ed. ISBN: 9781138423848 (CRC Press, 2012).

5. Handy, R. D. *et al.* Ecotoxicity test methods for engineered nanomaterials: Practical experiences and recommendations from the bench. *Environmental Toxicology and Chemistry* **31,** 15–31. ISSN: 07307268 (Jan. 2012).

6. Collin, B. *et al.* Environmental release, fate and ecotoxicological effects of manufactured ceria nanomaterials. *Environmental Science: Nano.* doi:`10.1039/c4en00149d` (2014).

7. Cassee, F. R. *et al.* Exposure, Health and Ecological Effects Review of Engineered Nanoscale Cerium and Cerium Oxide Associated with its Use as a Fuel Additive. *Critical Reviews in Toxicology* **41,** 213–229. ISSN: 1547-6898 (2011).

8. Jung, H., Kittelson, D. B. & Zachariah, M. R. The influence of a cerium additive on ultrafine diesel particle emissions and kinetics of oxidation. *Combustion and Flame* **142,** 276–288 (2005).

9. Costantini, M. G. *et al. Evaluation of Human Health Risk from Cerium Added to Diesel Fuel* tech. rep. (Health Effects Institute, Boston, USA, 2001).

10. Clark, A., Zhu, A., Sun, K. & Petty, H. R. Cerium oxide and platinum nanoparticles protect cells from oxidant-mediated apoptosis. *Journal of Nanoparticle Research* **13,** 5547–5555 (2011).

11. Brenner, S. The genetics of Caenorhabditis elegans. *Genetlcs* **77,** 71–94 (1974).

12. Warheit, D. B., Borm, P. J. A., Hennes, C. & Lademann, J. Testing strategies to establish the safety of nanomaterials: Conclusions of an ECETOC workshop. *Inhalation Toxicology* **19,** 631–643. ISSN: 08958378 (2007).

13. Menard, A., Drobne, D. & Jemec, A. *Ecotoxicity of nanosized TiO2. Review of in vivo data* Mar. 2011. doi:`10.1016/j.envpol.2010.11.027`. `http://www.ncbi.nlm.nih.gov/pubmed/21186069%20https://linkinghub.elsevier.com/retrieve/pii/S0269749110005385`.

14. Tiede, K., Hassellöv, M., Breitbarth, E., Chaudhry, Q. & Boxall, A. B. Considerations for environmental fate and ecotoxicity testing to support environmental risk assessments for engineered nanoparticles. *Journal of Chromatography A* **1216,** 503–509. ISSN: 00219673 (Jan. 2009).

15. Oberdörster, G., Oberdörster, E. & Oberdörster, J. Nanotoxicology: An emerging discipline evolving from studies of ultrafine particles. *Environmental Health Perspectives* **113,** 823–839. ISSN: 00916765 (2005).

16. Nørgaard Sørensen, S. & Baun, A. Controlling silver nanoparticle exposure in algal toxicity testing-A matter of timing. *Nanotoxicology* **ISSN,** 201–209 (2015).

17. Ramzan, M. *Effect of Surface Chemistry and Physical Properties of Carbon Nanotubes on the Adsorption of Polycyclic Aromatic Hydrocarbons in Aqueous Solutions* PhD thesis (Norwegian University of Science and Technology, Trondheim, 2013), 150.

18. Glomstad, B. *et al.* Carbon Nanotube Properties Influence Adsorption of Phenanthrene and Subsequent Bioavailability and Toxicity to Pseudokirchneriella subcapitata. *Environmental Science & Technology* **50,** 2660–2668 (Mar. 2016).

19. Glomstad, B. *et al.* Evaluation of methods to determine adsorption of polycyclic aromatic hydrocarbons to dispersed carbon nanotubes. *Environmental Science and Pollution Research* **24,** 23015–23025. ISSN: 0944-1344 (Oct. 2017).

20. Zindler, F. *et al.* Phenanthrene Bioavailability and Toxicity to Daphnia magna in the Presence of Carbon Nanotubes with Different Physicochemical Properties. *Environmental Science & Technology* **50,** 12446–12454 (Nov. 2016).

21. Nichols, G. *et al.* A Review of the Terms Agglomerate and Aggregate with a Recommendation for Nomenclature Used in Powder and Particle Characterization. *Journal of Pharmaceutical Sciences* **91,** 2103–2109. ISSN: 00223549 (Oct. 2002).

22. Nowack, B. & Bucheli, T. D. Occurrence, behavior and effects of nanoparticles in the environment. *Environmental pollution,* 5–22 (2007).

23. Chandra Ray, P., Yu &, H. & Fu, P. P. Toxicity and Environmental Risks of Nanomaterials: Challenges and Future Needs. *Journal of Environmental Science and Health* **27,** 1–35 (2009).

24. Johnston, B. D. *et al.* Bioavailability of nanoscale metal oxides TiO2, CeO2, and ZnO to fish. *Environmental Science and Technology* **44,** 1144–1151. ISSN: 0013936X (Feb. 2010).

25. Tyne, W., Lofts, S., Spurgeon, D. J., Jurkschat, K. & Svendseny, C. A new medium for caenorhabditis elegans toxicology and nanotoxicology studies designed to better reflect natural soil solution conditions setac. *Environ Toxicol Chem* **32,** 1711–1717 (2013).

26. Barcikowski, S. *et al.* Interaction of colloidal nanoparticles with their local environment: the (ionic) nanoenvironment around nanoparticles is different from bulk and determines the physico-chemical properties of the nanoparticles. *Interface.* doi:`10.1098/rsif.2013.0931` (2013).

27. Faure, B. *et al. Dispersion and surface functionalization of oxide nanoparticles for transparent photocatalytic and UV-protecting coatings and sunscreens* 2013. doi:`10.1088/1468-6996/14/2/023001`.

28. Hassellv, M. & Kaegi, R. in *Environmental and Human Health Impacts of Nanotechnology* 211–266 (John Wiley & Sons, Ltd, Chichester, UK). doi:`10.1002/9781444307504.ch6`.

29. Linsinger T *et al. Requirements on measurements for the implementation of the European Commission definition of the term 'nanomaterial'* 2012. doi:`10.2787/63490`.

30. Murphy, M. P. How mitochondria produce reactive oxygen species. *Biochemical Journal* **417,** 1–13. ISSN: 0264-6021 (Jan. 2008).

31. Lushchak, V. I. Free radicals, reactive oxygen species, oxidative stress and its classification. *Chemico-Biological Interactions* **224,** 164–175. ISSN: 18727786 (Dec. 2014).

32. Wu, G., Fang, Y.-Z., Yang, S., Lupton, J. R. & Turner, N. D. Glutathione metabolism and its implications for health. *The Journal of nutrition* **134,** 489–92. ISSN: 0022-3166 (Mar. 2004).

33. Braeckman, B., Back, P. U. & Matthijssens, F. in *Oxidative stress* (eds Olsen, A. & Gill, M. S.) (Cham, Switzerland Springer, 2017). ISBN: 9783319447018. `https://lib.ugent.be/catalog/pug01:8515541`.

34. Doonan, R. *et al.* Against the oxidative damage theory of aging: Superoxide dismutases protect against oxidative stress but have little or no effect on life span in Caenorhabditis elegans. *Genes and Development.* ISSN: 08909369. doi:`10.1101/gad.504808` (2008).

35. Braeckman, B. P., Smolders, A., Back, P. & De Henau, S. In Vivo Detection of Reactive Oxygen Species and Redox Status in Caenorhabditis elegans. *Antioxidants & Redox Signaling* **25,** 577–592. ISSN: 1523-0864 (2016).

36. McCord, J. M. & Fridovich, I. Superoxide dismutase. An enzymic function for erythrocuprein (hemocuprein). *Journal of Biological Chemistry* **244,** 6049–6055. ISSN: 00219258 (Nov. 1969).

37. Hoogewijs, D., Houthoofd, K., Matthijssens, F., Vandesompele, J. & Van-fleteren, J. R. Selection and validation of a set of reliable reference genes for quantitative sod gene expression analysis in C. elegans. *BMC Molecular Biology* **9,** 9. ISSN: 14712199 (Jan. 2008).

38. Esch, F. *et al.* Electron Localization Determines Defect Formation on Ceria Substrates. *Science* **74,** 53001 (1995).

39. Dutta, P. *et al.* Concentration of Ce3+ and Oxygen Vacancies in Cerium Oxide Nanoparticles. *Chemistry of materials.* doi:10.1021/cm061580n (2006).

40. Wu, L. *et al.* Oxidation state and lattice expansion of CeO2-x nanoparticles as a function of particle size. *Physical Review B* **69,** 125415. ISSN: 1098-0121 (2004).

41. Giese, B. *et al.* Risks, Release and Concentrations of Engineered Nano-material in the Environment. *Scientific Reports* **8,** 1565. ISSN: 2045-2322 (Dec. 2018).

42. Johnson, A. C. & Park, B. Predicting contamination by the fuel additive cerium oxide engineered nanoparticles within the United Kingdom and the associated risks. *Environmental Toxicology and Chemistry* **31,** 2582–2587. ISSN: 07307268 (Nov. 2012).

43. Lizon, C. & Fritsch, P. Chemical toxicity of some actinides and lanthanides towards alveolar macrophages: an in vitro study. *International journal of radiation biology* **75,** 1459–71. ISSN: 0955-3002 (Nov. 1999).

44. Paoli, L. *et al.* Uptake and acute toxicity of cerium in the lichen Xanthoria parietina. *Ecotoxicology and Environmental Safety* **104,** 379–385. ISSN: 10902414 (June 2014).

45. Wang, X. *et al.* Cerium toxicity, uptake and translocation in Arabidopsis thaliana seedlings. *Journal of Rare Earths* **30,** 579–585. ISSN: 10020721 (2012).

46. Du, X., Zhang, T., Li, R. & Wang, K. Nature of cerium(III)- and lanthanum(III)-induced aggregation of human erythrocyte membrane proteins. *Journal of inorganic biochemistry* **84,** 67–75. ISSN: 0162-0134 (Mar. 2001).

47. Shivakumar, K. & Nair, R. R. Cerium depresses protein synthesis in cultured cardiac myocytes and lung fibroblasts. *Molecular and cellular biochemistry* **100,** 91–6. ISSN: 0300-8177 (Jan. 1991).

48. Ma, Y. *et al.* Toxicity of cerium and thorium on Daphnia magna. *Ecotoxicology and Environmental Safety* **134,** 226–232. ISSN: 10902414 (Dec. 2016).

49. Johannesson, K. H., Stetzenbach, K. J., Hodge, V. F. & Berry Lyons, W. Rare earth element complexation behavior in circumneutral pH groundwaters: Assessing the role of carbonate and phosphate ions. *Earth and Planetary Science Letters* **145,** 139–141. ISSN: 0012821X (Mar. 1996).

50. Wells, W. H. & Wells, V. L. in *Patty's Toxicology* 817–840 (John Wiley & Sons, Inc., Hoboken, NJ, USA, Jan. 2012). doi:`10.1002/0471435139.tox043.pub2`. `http://doi.wiley.com/10.1002/0471435139.tox043.pub2`.

51. Firsching, F. H. & Mohammadzadel, J. Solubility Products of the Rare-Earth Carbonates. *Journal of Chemical and Engineering Data* **31,** 40–42. ISSN: 15205134 (Jan. 1986).

52. Barry, M. J. & Meehan, B. J. The acute and chronic toxicity of lanthanum to Daphnia carinata. *Chemosphere* **41,** 1669–1674. ISSN: 00456535 (Nov. 2000).

53. Ciofani, G., Genchi, G. G., Mazzolai, B. & Mattoli, V. Transcriptional profile of genes involved in oxidative stress and antioxidant defense in PC12 cells following treatment with cerium oxide nanoparticles. *Biochimica et Biophysica Acta - General Subjects* **1840,** 495–506. ISSN: 03044165 (2014).

54. Heckert, E. G., Karakoti, A. S., Seal, S. & Self, W. T. The role of cerium redox state in the SOD mimetic activity of nanoceria. *Biomaterials* **29,** 2705–2709. ISSN: 01429612 (June 2008).

55. Grulke, E. *et al.* Nanoceria: factors affecting its pro- and anti-oxidant properties. *Environ. Sci.: Nano* **1,** 429–444. ISSN: 2051-8153 (Aug. 2014).

56. Lahive, E. *et al.* Toxicity of cerium oxide nanoparticles to the earthworm Eisenia fetida: subtle effects. *Environmental Chemistry* **11,** 268–278 (2014).

57. Lin, W., Huang, Y.-W., Zhou, X.-D. & Ma, Y. Toxicity of Cerium Oxide Nanoparticles in Human Lung Cancer Cells. *International Journal of Toxicology* **25,** 451–457. ISSN: 1091-5818 (2006).

58. Zhang, H. *et al.* Nano-CeO 2 Exhibits Adverse Effects at Environmental Relevant Concentrations. *Environ. Sci. Technol* **45,** 3725–3730 (2011).

59. Arnold, M. C., Badireddy, A. R., Wiesner, M. R., Di Giulio, R. T. & Meyer, J. N. Cerium Oxide Nanoparticles are More Toxic than Equimolar Bulk Cerium Oxide in Caenorhabditis elegans. *Archives of Environmental Contamination and Toxicology* **65,** 224–233. ISSN: 0090-4341 (Aug. 2013).

60. Penney, E. B. & Mccabe, B. D. Parkinson's Disease: Insights from Invertebrates. *Parkinson's Disease,* 321–333 (Jan. 2008).

61. Barr, M. M. Super models. *Physiol Genomics* **13,** 15–24 (2003).

62. Riddle, D. L., Blumenthal, T., Meyer, B. J. & Priess, J. R. *C. elegans II* ISBN: 9780879695323 (Cold Spring Harbor Laboratory Press, 1997).

63. Fielenbach, N. & Antebi, A. C. elegans dauer formation and the molecular basis of plasticity. *Genes and development,* 2149–2165 (2008).

64. Altun, Z. F. & Hall, D. H. *WormAtlas: Handbook of C. elegans Anatomy* 2012.

65. Hirsh, D., Oppenheim, D. & Klass, M. *Development of the Reproductive System of Caenorhabditis elegans* tech. rep. (1976), 200–219.

66. McGhee, J. & Ghafouri, S. Bacterial residence time in the intestine of Caenorhabditis elegans. *Nematology* **9,** 87–91. ISSN: 1388-5545 (Jan. 2007).

67. The C. elegans Sequencing Consortium. Genome Sequence of the Nematode C. elegans: A Platform for Investigating Biology. *Science* **282,** 2012–2018 (1998).

68. Back, P. *et al.* Exploring real-time in vivo redox biology of developing and aging Caenorhabditis elegans. *Free Radical Biology and Medicine* **52,** 850–859. ISSN: 08915849 (2012).

69. Murphy, D. B. *Fundamentals of light microscopy and and electronic imaging* tech. rep. (2001), 385. http://www.biology.uoc.gr/courses/BIOL493/documents/book.pdf.

70. Lichtman, J. W. & Conchello, J.-A. Fluorescence microscopy. *Nature Methods* **2,** 910–919. ISSN: 1548-7091 (Dec. 2005).

71. JoVE Science Education Database. *Introduction to Fluorescence Microscopy* https://www.jove.com/science-education/5040/introduction-to-fluorescence-microscopy (JoVE, Cambridge, 2019).

72. Colding-Christensen, C. S. *Fluorescence Microscopy - the Magic of Fluorophores and Filters - Bitesize Bio* https://bitesizebio.com/33529/fluorescence-microscopy-the-magic-of-fluorophores-and-filters/ (2019).

73. Shashkova, S. & Leake, M. C. Single-molecule fluorescence microscopy review: shedding new light on old problems. *Bioscience Reports* **37,** 20170031 (2017).

74. Prasher, D. C., Eckenrode, V. K., Ward, W. W., Prendergast, F. G. & Cormier, M. J. Primary structure of the Aequorea victoria green-fluorescent protein. *Gene* **111,** 229–33. ISSN: 0378-1119 (Feb. 1992).

75. Chalfie, M., Tu, Y., Euskirchen, G., Ward, W. W. & Prasher, D. C. Green fluorescent protein as a marker for gene expression. *Science (New York, N.Y.)* **263,** 802–805 (Feb. 1994).

76. Tsien, R. Y. *The green fluorescent protein* tech. rep. (Howard Hughes Medical Institute, San Diego, 1998), 509–553. www.annualreviews.org.

77. Williams, D. B. & Carter, C. B. *Transmission Electron Microscopy: A Textbook for Materials Science* 2nd ed. (Springer, 2009).

78. Walton, W. H. *Feret's statistical diameter as a measure of particle size* Aug. 1948. doi:10.1038/162329b0. http://www.nature.com/articles/162329b0.

79. Malvern Instruments. *Zetasizer Nano user manual* tech. rep. (2013).

80. Filipe, V., Hawe, A. & Jiskoot, W. Critical evaluation of nanoparticle tracking analysis (NTA) by NanoSight for the measurement of nanoparticles and protein aggregates. *Pharmaceutical Research* **27,** 796–810. ISSN: 07248741 (May 2010).

81. Jarzębski, M. *et al.* Particle tracking analysis in food and hydrocolloids investigations. *Food Hydrocolloids* **68,** 90–101. ISSN: 0268005X (July 2017).

82. Abou-Shakra, F. R. Biomedical applications of inductively coupled plasma mass spectrometry (ICP–MS) as an element specific detector for chromatographic separations. *Handbook of Analytical Separations* **4,** 351–371 (2003).

83. Barberá, R., Farré, R. & Lagarda, M. Copper: Properties and Determination. *Encyclopedia of Food Sciences and Nutrition,* 1634–1639 (2003).

84. Godfrey, L. V. & Glass, J. B. The Geochemical Record of the Ancient Nitrogen Cycle, Nitrogen Isotopes, and Metal Cofactors. *Methods in Enzymology* **486,** 483–506. ISSN: 0076-6879 (Jan. 2011).

85. Singh, A. K. & Singh, A. K. Experimental Methodologies for the Characterization of Nanoparticles. *Engineered Nanoparticles,* 125–170 (Jan. 2016).

86. Aceto, M. in *Advances in Food Traceability Techniques and Technologies: Improving Quality Throughout the Food Chain* 137–164 (Woodhead Publishing, Jan. 2016). ISBN: 9780081003213. doi:10 . 1016 / B978 - 0 - 08 - 100310 - 7 . 00008 - 9. https : / / www . sciencedirect . com / science / article/pii/B9780081003107000089.

87. ISO/TC 147/SC 5. *ISO 10872:2010 Water quality - Determination of the toxic effect of sediment and soil samples on growth, fertility and reproduction of Caenorhabditis elegans (Nematoda)* 2010. (2018).

88. Handy, R. D. *et al.* The ecotoxicology and chemistry of manufactured nanoparticles. *Ecotoxicology* **17,** 287–314 (2008).

89. Patil, S., Sandberg, A., Heckert, E., Self, W. & Seal, S. Protein adsorption and cellular uptake of cerium oxide nanoparticles as a function of zeta potential. *Biomaterials* **28,** 4600–4607 (2007).

90. Kosmulski, M. The pH-dependent surface charging and the points of zero charge. *Journal of Colloid and Interface Science* **253,** 77–87. ISSN: 00219797 (Sept. 2002).

91. Van Hoecke, K., De Schamphelaere, K. A. C., Van Der Meeren, P., Smagghe, G. & Janssen, C. R. Aggregation and ecotoxicity of CeO2 nanoparticles in synthetic and natural waters with variable pH, organic matter concentration and ionic strength. *Environmental Pollution* **159,** 970–976 (2011).

92. Calabrese, E. J. & Baldwin, L. A. Defining hormesis. *Human and Experimental Toxicology* **21,** 91–97. ISSN: 09603271 (Feb. 2002).

93. Mattson, M. P. *Hormesis defined* Jan. 2008. doi:`10.1016/j.arr.2007.08.007`. `https://www.sciencedirect.com/science/article/pii/S1568163707000712`.

94. NANoREG. *Accumulation potential and aquatic toxicity of relevant groups of nanomaterials and product formula* tech. rep. 310584 (2016), 127. `https://www.rivm.nl/sites/default/files/2019-01/NANoREG%7B%5C_%7DD4%7B%5C_%7D12%7B%5C_%7DR%7B%5C_%7DAccumulation%7B%5C_%7Dpotential%7B%5C_%7Dand%7B%5C_%7Daquatic%7B%5C_%7Dtoxicity%7B%5C_%7Dof%7B%5C_%7Drelevant%7B%5C_%7Dgroups%7B%5C_%7Dof%7B%5C_%7Dnanomaterials%7B%5C_%7Dand%7B%5C_%7Dproduct%7B%5C_%7Dformula.pdf`.

95. Kawagoe, M. *et al.* Orally administrated rare earth element cerium induces metallothionein synthesis and increases glutathione in the mouse liver. *Life Sciences* **77,** 922–937. ISSN: 00243205 (July 2005).

96. Back, P., Braeckman, B. P. & Matthijssens, F. ROS in Aging Caenorhabditis elegans : Damage or Signaling? *Oxidative Medicine and Cellular Longevity* **2012,** 1–14. ISSN: 1942-0900 (2012).

97. Aller, I., Rouhier, N. & Meyer, A. J. Development of roGFP2-derived redox probes for measurement of the glutathione redox potential in the cytosol of severely glutathione-deficient rml1 seedlings. *Frontiers in Plant Science* **4,** 506. ISSN: 1664-462X (2013).

98. Das, T., Sharma, A. & Talukder, G. *Effects of lanthanum in cellular systems - A review* Dec. 1988. doi:`10.1007/BF02917504`. `http://link.springer.com/10.1007/BF02917504`.

99. Sinclair, J. & Hamza, I. Lessons from bloodless worms: Heme homeostasis in C. elegans. *BioMetals* **28,** 481–489. ISSN: 15728773 (2015).

100. Roh, J.-Y., Park, Y.-K., Park, K. & Choi, J. Ecotoxicological investigation of CeO2 and TiO2 nanoparticles on the soil nematode Caenorhabditis elegans using gene expression, growth, fertility, and survival as endpoints. *Environmental Toxicology and Pharmacology* **29,** 167–172 (2010).

101. Rogers, N., Batley, G. E., Angel, B. M. & Baalousha, M. Physico-chemical behaviour and algal toxicity of nanoparticulate CeO. *Environmental chemistry,* 50–60 (2010).

102. Van Hoecke, K. *et al.* Fate and Effects of CeO 2 Nanoparticles in Aquatic Ecotoxicity Tests. *Environ. Sci. Technol.* 4537–4546 (2009).

103. Ledwich, D., Wu, Y.-C., Driscoll, M. & Xue, D. *Methods for the Study of Programmed Cell Death in the Nematode Caenorhabditis elegans* tech. rep. (Department of Molecular, Cellular, and Developmental Biology, Colorado).

104. Bloch Hartmann, N. *Ecotoxicity of engineered nanoparticles to freshwater organisms* tech. rep. (Technical University of Denmark, Copenhagen, 2011), 91. `http://orbit.dtu.dk/ws/files/5598471/Nanna%20I%20B% 20Hartmann%20PhD-thesis%20WWW-Version.pdf`.

105. Žutić, V. & Svetličić, V. in *Marine Chemistry* 149–165 (Springer-Verlag, Berlin/Heidelberg, 2005). doi:`10.1007/10683826_6`. `http://link. springer.com/10.1007/10683826%7B%5C_%7D6`.

106. Van Hoecke, K., De Schamphelaere, K. A. C., Van der Meeren, P., Lucas, S. & Janssen, C. R. Ecotoxicity of silica nanoparticles to the green alga Pseudokirchneriella subcapitata: importance of surface area. *Environmental toxicology and chemistry* **27,** 1948–57 (Sept. 2008).

107. Baun, A., Hartmann, N. B., Grieger, K. D. & Hansen, S. F. *Setting the limits for engineered nanoparticles in European surface waters - Are current approaches appropriate?* Oct. 2009. doi:`10.1039/b909730a`. `http://www. ncbi.nlm.nih.gov/pubmed/19809700%20http://xlink.rsc.org/?DOI= b909730a`.

108. Oberdörster, G., Oberdörster, E. & Oberdörster, J. Concepts of Nanoparticle Dose Metric and Response Metric. *Environmental Health Perspectives* **115,** A290 (2007).

109. Petersen, E. J., Akkanen, J., Kukkonen, J. V. & Weber, W. J. Biological uptake and depuration of carbon nanotubes by daphnia magna. *Environmental Science and Technology* **43,** 2969–2975. ISSN: 0013936X (Apr. 2009).

110. Koukal, B. *et al.* Effect of Pseudokirchneriella subcapitata (Chlorophyceae) exudates on metal toxicity and colloid aggregation. *Water Research* **41,** 63–70. ISSN: 00431354 (Jan. 2007).

111. Miao, A. J. *et al.* The algal toxicity of silver engineered nanoparticles and detoxification by exopolymeric substances. *Environmental Pollution* **157,** 3034–3041. ISSN: 02697491 (Nov. 2009).

112. Hall, S., Bradley, T., Moore, J. T., Kuykindall, T. & Minella, L. Acute and chronic toxicity of nano-scale TiO2 particles to freshwater fish, cladocerans, and green algae, and effects of organic and inorganic substrate on TiO2 toxicity. *Nanotoxicology* **3,** 91–97. ISSN: 17435390 (Jan. 2009).

# Appendix A  Drift corrections

When performing ICP-MS measurements, the 20 µg/L cerim standard was measured repeatedly every 10 samples to permit post-measurement drift corrections. This was done by multiplying all results with 20 µg/L and dividing by the mean of the two nearest standard measurements, as in the following example. 4 significant numbers are included for illustrative purposes.

In one of the diluted samples, the concentration was measured to be 7.432 µg/L. The concentration of the two nearest standard measurements performed before and after this sample were measured to be 19.96 and 20.00 µg/L, respectively. The corrected concentration $C_c$ for the replicate of interest was calculated as follows:

$$C_c = \frac{7.432\,\text{µg/L} \times 20\,\text{µg/L}}{\frac{19.96\,\text{µg/L}+20.00\,\text{µg/L}}{2}} = 7.439\,\text{µg/L} \tag{6}$$

Corrections were performed on all measurements, and the corrected values used in further analysis.

# Appendix B  TEM micrographs

Transmission electron microscopy (TEM) micrographs of $CeO_2$ NPs were taken during the project thesis. The protocol in section 3.1 was used to prepare the NP suspensions in $ddH_2O$ and MHRW T. The NP suspension in ethanol was prepared by briefly vortexing a $1\,mg/mL$ suspension, and immediately using it to prepare the grids. Example micrographs are shown in figure 23.
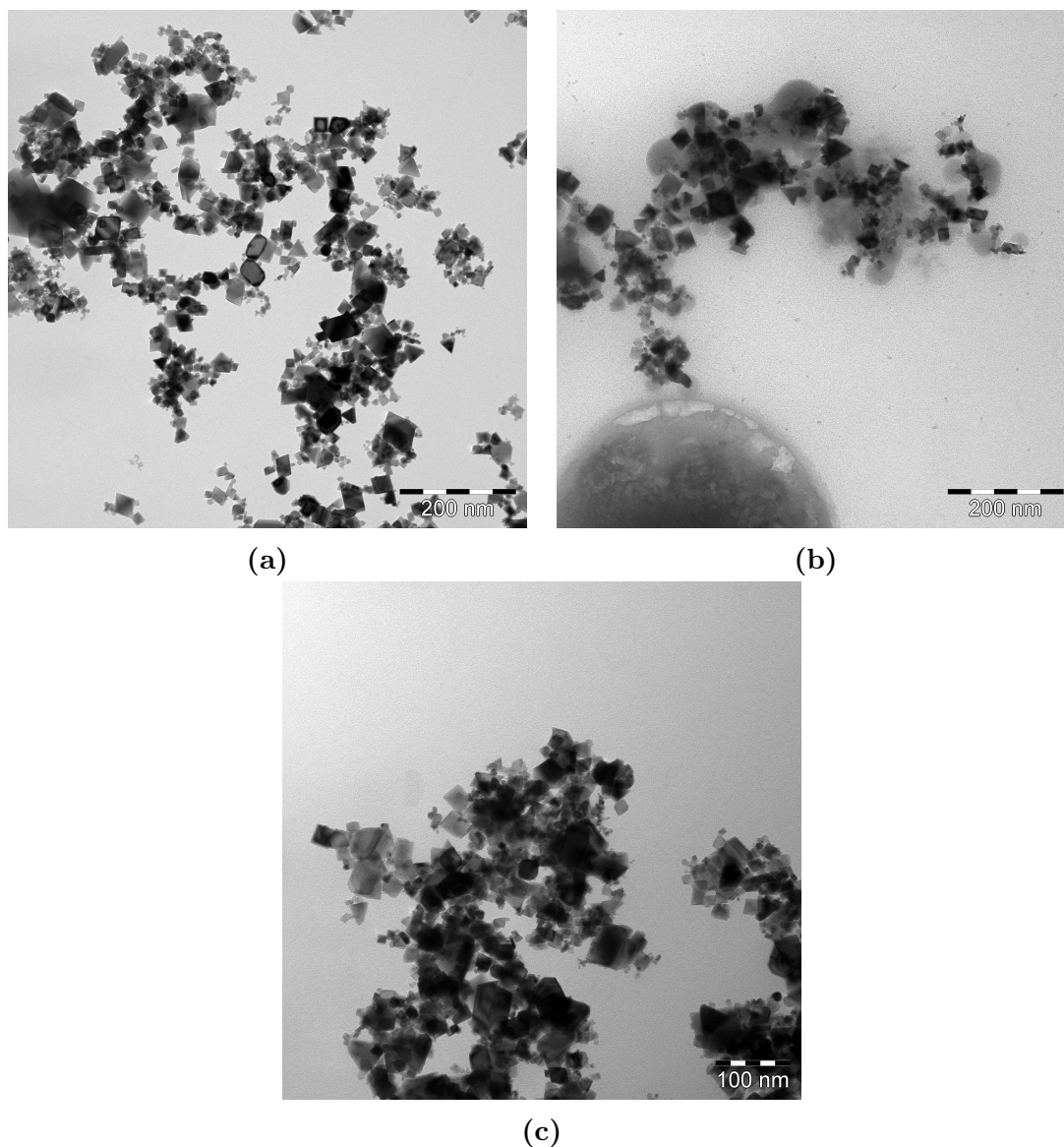


(a)



(b)



(c)

**Figure 23:** Transmission electron microscopy (TEM) micrographs of $CeO_2$ nanoparticles. (a) $0.1\,g/L$ NPs in $ddH_2O$, (b) $0.1\,g/L$ NPs in MHRW T and (c) $1\,g/L$ NPs in ethanol.

# Appendix C   ICP-MS results from E2

The ICP-MS results from E2 are shown in table 5. All three treatments with $CeO_2$ NPs show at least a 50 % reduction in cerium concentration from t=0 h to t=96 h.

**Table 5:** Cerium concentration (mean $\pm$ 1 standard deviation) in the exposure media for E2, measured by ICP-MS. N=3, each replicate was measured $10 \times 1$ second.

| Exposure | Estimated concentration (mg/L) | Measured concentration at t=0 h (mg/L) | Measured concentration at t=96 h (mg/L) |
|---|---|---|---|
| $CeO_2$ NPs | 0.59 | $0.47 \pm 0.029$ | $0.22 \pm 0.022$ |
| | 4.7 | $3.93 \pm 0.058$ | $1.48 \pm 0.012$ |
| | 38 | $33 \pm 1.7$ | $16 \pm 1.3$ |
| $Ce(NO_3)_3$ | 0.32 | $0.270 \pm 0.0056$ | $0.236 \pm 0.014$ |
| | 3.0 | $2.49 \pm 0.016$ | $2.1 \pm 0.12$ |
| | 44 | $40 \pm 1.0$ | $38 \pm 2.1$ |

# Appendix D  Dose-response for E1 and E3

Two toxicity tests with the same setup was performed 6 months apart, E1 during the project work and E3 during the current work. Figure 24 show the toxic effect on the nematode fertility and reproduction after exposure to $Ce(NO_3)_3$ for the two experiments.



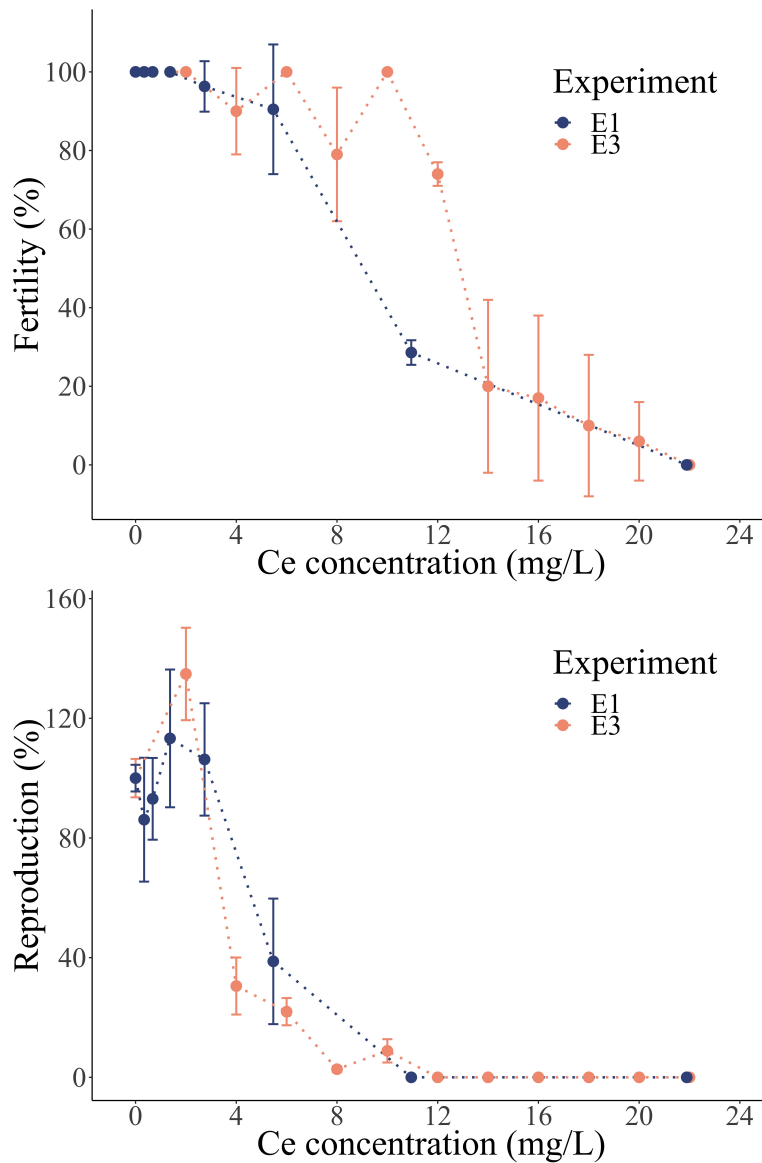**Figure 24:** Dose-response curves for fertility (top) and reproduction (bottom) for N2 nematodes after exposure to $Ce(NO_3)_3$ in a 96 h chronic toxicity test for two experiments (E1 and E3). The results are normalized to the control for direct comparison.